LA-UR-23-32864

Approved for public release; distribution is unlimited.

Title:	Summary of Gas Generation Behavior Observed in 3013 Surveillance and Monitoring Program Shelf-Life Experiments
Author(s):	Narlesky, Joshua Edward Veirs, Douglas Kirk
Intended for:	Reference document for DOE-STD-3013 currently in RevCom Report
Issued:	2024-09-17 (rev.1)

Summary of Gas Generation Behavior Observed in 3013 Surveillance and Monitoring Program Shelf-Life Experiments

Joshua E. Narlesky
Douglas Kirk Veirs

September 13, 2024

Los Alamos
NATIONAL LABORATORY

Contents

Figures

Contents

Contents

Tables

Abstract

Gas generation experiments have been conducted in small- and full-scale test containers at Los Alamos National Laboratory on samples of plutonium oxide material collected from plutonium processes across the DOE complex and tested at the bounding conditions for the Department of Energy 3013 Standard. The gas composition and pressures in the sealed experimental containers were measured over periods of months to years. These experiments have provided results for the formation and consumption of hydrogen and other gases. The conditions supporting the formation of flammable gas mixtures of hydrogen and oxygen in flammable gas mixtures were also determined. Different behaviors were observed between the materials tested based on their compositions, the stabilization performed on the material, and the post-stabilization handling of the material. Many of the experiments are still ongoing. This report summarizes the results obtained for the gas generation behavior for high-purity plutonium oxides and salt-bearing impure plutonium oxides in sealed containers.

1 Introduction

In 1994 the Department of Energy released the 3013 Standard with the title, “Criteria for safe storage of plutonium metals and oxides”, DOE-STD-3013-94.[1] The pressure equation in the standard was based on a bounding assumption of “100% radiolysis of retained moisture” to hydrogen and oxygen”. This assumption was later revised in the 1996 revision to state that water radiolysis would produce hydrogen but not oxygen.[2] In 1999 the 3013 Standard was further revised and stated that the assumption of complete radiolysis of adsorbed water to form hydrogen was not observed in a variety of environments involving sealed containers and that “the bounding gas assumption made in this Standard is highly conservative”.[3] There was evidence that “actual maximum pressures under 100 psig are likely”, but the conditions and veracity of data was of concern.[4]

The MIS Program was introduced in Appendix A of DOE-STD-3013-99. with the goal of providing experimental evidence under controlled conditions of the magnitude of the hydrogen generation, the consumption of oxygen, the magnitude of other gases such as carbon dioxide, and the maximum pressures that could be generated in actual 3013 containers while in storage.[3] The MIS Program initiated shelf-life studies to determine the pressure and composition of the gases generated when these materials are stored in sealed containers over periods of months to years. Experiments were conducted with full-scale and small-scale test containers referred to as small-scale reactors (SSRs). These experiments have been ongoing since 2003.

The MIS shelf-life studies with materials loaded in full-scale containers are hereinafter referred to as the large-scale shelf-life studies or large-scale experiments.[5, 6] These experiments replicate the exact geometry of the materials packaged in 3013 inner containers, but the number of full-scale tests was limited due to the amount of material required. Since 2003, twelve large-scale experiments were loaded with chloride-bearing Pu oxides for corrosion studies, and two large-scale experiments were loaded with high-purity oxides for the purpose of conducting thermal conductivity studies and to investigate the formation and consumption of hydrogen and the consumption of water.[7,8] The experimental details for the large-scale experiments are given in Appendix A:. Each experiment provided pressure, temperature, and gas composition measurements. The large-scale experiments also had the capability of measuring water vapor pressure by Raman spectroscopy or from relative humidity measurements (RH) obtained with RH sensors installed in the containers.

The small-scale experiments were conducted with the SSRs in the small-scale array, which allows the simultaneous testing of up to 45 individual samples and allowed the testing of the full range of MIS represented materials. The SSRs were refined to a scale 1/500th the size a 3013 inner container by volume. Each SSR was loaded with nominally 10 grams of material, and water was added to the material by vapor adsorption to reach the 3013 Standard limit of 0.5 wt.%. The SSRs were monitored continuously, and gas sampling was performed periodically to determine the gas generation behavior over long periods of time. Since 2003, over 280 small-scale experiments have been initiated. This includes 45 MIS Represented materials, some of which have been loaded into multiple SSRs. The experimental details for the small-scale experiments are given in Appendix B:. The interim results showed that to understand the effects of all the variables—the amount of water, the specific power of the material, the specific surface area of the material, and the chloride concentration and composition—tests with prepared materials designed to probe the variable space would require 200 additional SSRs being loaded. Final reports have been completed on thirteen of the materials and are listed in Appendix B:.

Experimental

Very different behaviors are observed between materials with different classes of compositions. The behavior of the materials in shelf-life experiments can be mapped to actual materials in storage through representation, whereby these materials were expected to "reasonably predict the behavior of the material in storage for 50 years".[9] However, trends observed in the gas generation behavior allow the materials to be grouped more generally in to three classes: high-purity oxides, salt-bearing impure oxides, and non-salt impure oxides.[10] High-purity oxides and the subgroup high-purity mixed Pu-U oxides have an actinide content of 85% or greater. When calcined to 950 °C, these materials have a low specific surface area (typically 1 m^2 g^{-1} or lower) and a very low capacity for moisture adsorption. In storage experiments, these materials generate less than 10 kPa of hydrogen and no other gases.[11-21] However, these materials can generate much higher amounts of hydrogen and in some cases oxygen, carbon dioxide and nitrogen when packaging is deferred for periods of weeks to years after calcination to 950 °C or if the materials are calcined at temperatures lower than 950 °C.[15, 19, 21-23] Impure oxides are considered to be Pu oxide materials with an actinide content less than 85%. This group was subdivided into salt-bearing impure oxides, which have a chlorine content of 1% or greater and non-salt-bearing impure oxides. The salts in the impure oxides increase the moisture adsorption capacity well beyond that of Pu oxide alone and generate mostly hydrogen (typically greater than 10 kPa) in these studies.[10, 24, 25] The remainder of the impure materials include the non-salt-bearing impure oxides that generate much less hydrogen than those with chloride salts.

This report summarizes the key behaviors observed in high-purity oxide and salt-bearing impure oxides from a selection of the materials loaded in small- and large-scale experiments. The materials have a broad range of specific power, specific surface area, and impurity composition. Data from these experiments show the pressures generated inside sealed containers with plutonium oxide with bounding amounts of water, the formation of and consumption of hydrogen, oxygen, and other gases and the consumption of water. Some experiments have reached completion and have undergone destructive evaluation while others are still in progress. The materials described in this report are listed in the Appendices. Characterization data for each of the MIS represented samples is reported elsewhere.[26]

2 Experimental

To date, 14 large-scale containers have been loaded with various materials. A complete list of the large-scale experiments, materials, and added moisture is given in Appendix A: Table 4. The large-scale containers are instrumented with thermocouples and a pressure transducer. Containers loaded and installed in 2009 and later are also instrumented with RH sensors. Measurements of pressure, temperature, and RH (where equipped) are recorded every 15 minutes. All large-scale containers are connected to a gas manifold that is used to extract 5-mL gas samples for gas chromatography (GC). The GC is calibrated for helium, hydrogen, nitrogen, oxygen, carbon dioxide, carbon monoxide, and nitrous oxide. Large-scale containers installed prior to 2009 were equipped with Raman chambers to conduct *in situ* measurements of the same gases except for helium. Raman spectroscopy also provides a measurement of water vapor in containers that were not equipped with RH sensors. The temperature inside large-scale containers was not actively controlled but dependent on the decay heat of the loaded material. Containers in the LS Corrosion Series II had fiberglass insulation surrounding the container to allow the material to generate warmer conditions similar to those in a 9975 shipping container.

Over 280 small-scale experiments have been initiated at the time of writing this report. A complete list of the 45 MIS represented samples and their loading conditions is given in Appendix B:, Table 6. The loading conditions for the MIS represented materials targeted a moisture content of 0.5 wt. %. Additional

high-purity oxide materials were loaded with varying calcination conditions, specific surface area, specific power, and moisture. Nominally 10-g samples are loaded and sealed into SSRs with Conflat flange lids instrumented with pressure transducers. The SSRs were placed in a heated array maintained at 55 °C, a temperature which a 3013 container filled with oxide might generate. Some later experiments were conducted at room temperature to reduce the effect of thermal gradients between the top and bottom of the SSR. Measurements of the SSR pressure and the array temperature were recorded every 15 minutes by the data acquisition system. The gas manifold was used to extract 50-µL gas samples for GC measurements. The GC is calibrated for helium, hydrogen, nitrogen, oxygen, carbon dioxide, carbon monoxide, nitrous oxide, and nitric oxide. The experiments with MIS Represented materials continued until the gas composition showed no change over a period of at least 6 months after which they were removed from the array following the approval of the MIS Working Group. Upon removal, a measurement of the RH inside the SSR was performed using a lid fitted with a Vaisala HMT333 RH probe. Following the RH measurement, a sample of the material was split for a final moisture measurement by loss on heating to 200 °C. The inner bucket that held the material inside the SSR was emptied, cut apart, and cleaned in an ultrasonic cleaner, and examined by optical microscopy.

An ongoing series of experiments with high-purity Pu oxides exposed to a high RH environment is providing data to inform mechanisms for the formation and consumption of hydrogen and the consumption of water in sealed containers.[27, 28] These experiments, referred to as the RH studies, used samples of high-purity Pu oxides with varying specific power, specific surface area, and moisture content shown in Table 1. The variation in the specific surface area for the aqueous derived oxide was achieved by using material that had been originally calcined at different temperatures. Because the materials were stored in air following the original calcination, the materials were all heated to 400 °C to remove adsorbed species (water, carbon dioxide, and NO_x). The materials were then exposed to a humid environment for one week before they were transferred to a SSR with a RH sensor. These SSRs were installed in the unheated portion of the array that fluctuated with the temperature of the glovebox, approximately 28 to 30 °C. In addition to the pressure and array temperature, measurements of RH, water vapor pressure, and headspace temperature were recorded every 15 minutes by the data acquisition system. SSRs for the high-purity oxide experiment were removed from the array when the either the hydrogen was completely consumed or when it reached a stable equilibrium. Destructive evaluation was not performed on the high-purity oxide SSRs used in the RH studies.

Table 1. High-Purity Pu Oxides Used in the RH Studies.[27, 28]

Material	Process of Origin	$^{239}Pu/_{Pu}$ %	$^{239}Pu/_{Pu}$ %	^{241}Am (wt. %)	SP (w/kg)	SSA (m2 g-1)	Original Calcination Temperature
PEOF	Oxalate precipitation process	93.8	6.1	0.07	2.1	1.1	950 °C
MISSTD	Oxalate precipitation process	93.5	6.3	0.15	2.1	21.5	600 °C
LAO	Peroxide precipitation process	82.7	16.6	1.1	4.0	8.2	750 °C
BLO	Oxalate precipitation process	79.8	17.8	7.1	14.2	5.0	950 °C
BLO-C	Oxalate precipitation process	79.8	17.8	7.1	14.2	0.8	950 °C
AAPOX	Metal Oxidation	87.2	5.8	0.28	33.5	2.8	Unknown

3 Results

Analysis of data collected from the various shelf-life experiments has shown differences in behavior between high-purity Pu oxides, chloride-bearing impure oxides, and non-chloride-bearing impure oxides. The major differences between the groups is seen in the maximum pressures of the hydrogen generated, the time for hydrogen to reach its maximum pressure, and the time required for the hydrogen to decrease from its maximum toward an equilibrium value or toward zero. The groups of materials also show differences in the behavior of the other gases including oxygen, nitrogen, carbon dioxide, nitrous oxide and carbon monoxide. The behavior of the high-purity oxides and salt-bearing materials are described in the sections below. The behavior of the non-salt-bearing impure oxides are bounded by the salt-bearing impure oxides and are not included in this report.

3.1 High-Purity Oxides

The high-purity oxide group includes three subgroups: the RH study materials, MIS Represented high-purity Pu oxides, and MIS Represented mixed Pu-U high-purity oxides. The key observations from shelf-life experiments with high-purity Pu oxides include the following:

1) The primary gas generation behavior of high purity oxides is described by models that include the formation and consumption of hydrogen produced by the radiolysis of water adsorbed on the oxide surface.

2) Oxygen generation is observed in some high-purity oxides where the initial rate of hydrogen generation when normalized to the specific power exceeds 0.03 kPa day^{-1} W^{-1}.

3) The partial pressures of other gases including carbon dioxide and nitrogen exceed the maximum hydrogen partial pressure in materials aged in air for months to years after calcination.

The first group considered here are the materials in the RH studies, which show the behavior of hydrogen formation and consumption unaffected by impurities and adsorbed species other than water. The materials in the RH studies were selected based on their specific surface area and specific power. Calcining the material is known to reduce the specific surface area of high-purity Pu oxides especially at temperatures above 600 °C, but it is necessary for cleaning the surface of the oxide to remove water and other adsorbed species such as carbon dioxide and NO_x.[29] Therefore, the materials used in the RH studies were heated to at least 400 °C to clean the surface prior to loading. MISSTD and LAO materials were recalcined at their original calcination temperatures, 600 °C and 750 °C, respectively, which leaves the specific surface area of those materials unchanged. Therefore, carbon dioxide, nitrous oxide and carbon monoxide were not observed in the RH studies above trace levels. Although these materials do not meet the stabilization requirements for packaging under the 3013 Standard, the behavior of the hydrogen and other gases is relevant to high temperature stabilized material and should be considered bounding of any materials packaged in 3013 containers.

Figure 1 shows the partial pressures of the hydrogen and oxygen as a function of time for the RH study materials following exposure to 55% RH for one week prior to loading in the SSRs. Materials with higher specific power (BLO, BLO-C, and AAPOX) reached the maximum hydrogen pressure faster than the other materials. The BLO and MISSTD materials had the highest hydrogen pressures. Both materials had a specific surface area of at least 5 m^2 g^{-1}, which increased the capacity and the amount of adsorbed water

on the surface of the oxides. The BLO material had the highest initial rate of hydrogen production and reached its maximum pressure faster than the MISSTD material. The BLO material also had a higher maximum pressure than the MISSTD material, which had double the amount of adsorbed water under the same loading conditions. Both materials also generated a flammable hydrogen-oxygen gas mixture. Oxygen was consumed in all the other materials exposed to the same initial RH.

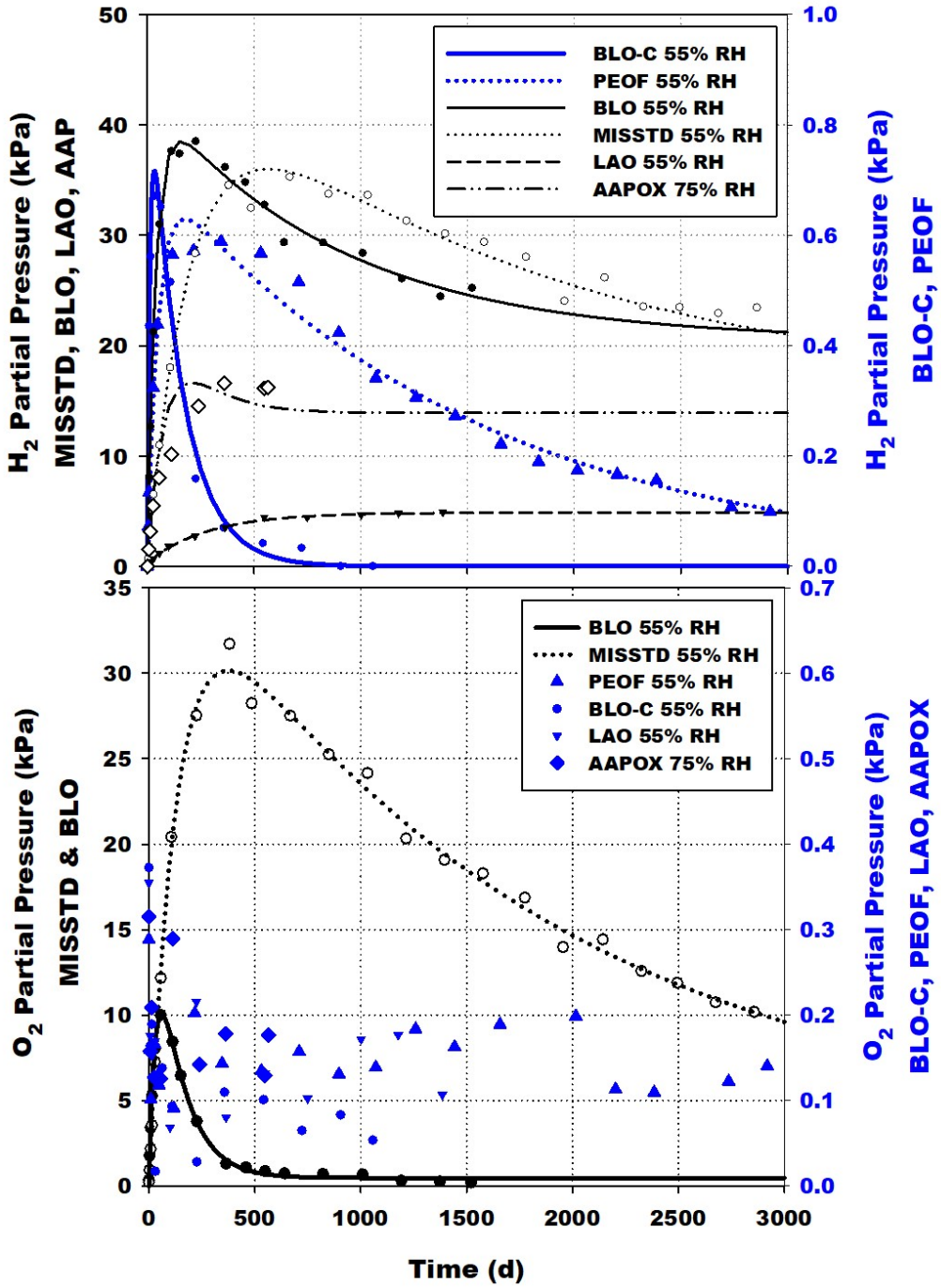

Figure 1. Partial pressures of hydrogen and oxygen as a function of time for six high-purity oxides exposed to high RH for one week.

Results

Differences in the behavior of the materials is strongly influenced by the specific power showing that the hydrogen (and oxygen) gas generation and consumption is dependent on the alpha radiation dose to the water. The hydrogen behavior of two materials calcined to 950 °C, PEOF in green and BLO-C in blue, are shown in Figure 2. Both materials have the same specific surface area, but different specific power. Three samples of each of the materials were loaded following exposure to three different RH, nominally 33%, 55% and 75% RH for one week. The exposure to the three different RH resulted in slightly different amounts of water loaded on each of the samples. For each water loading, the BLO-C material had a higher initial rate of hydrogen formation and a higher maximum pressure than the PEOF material loaded under the same conditions. The BLO-C material also decreased to zero faster than the low specific power PEOF material.

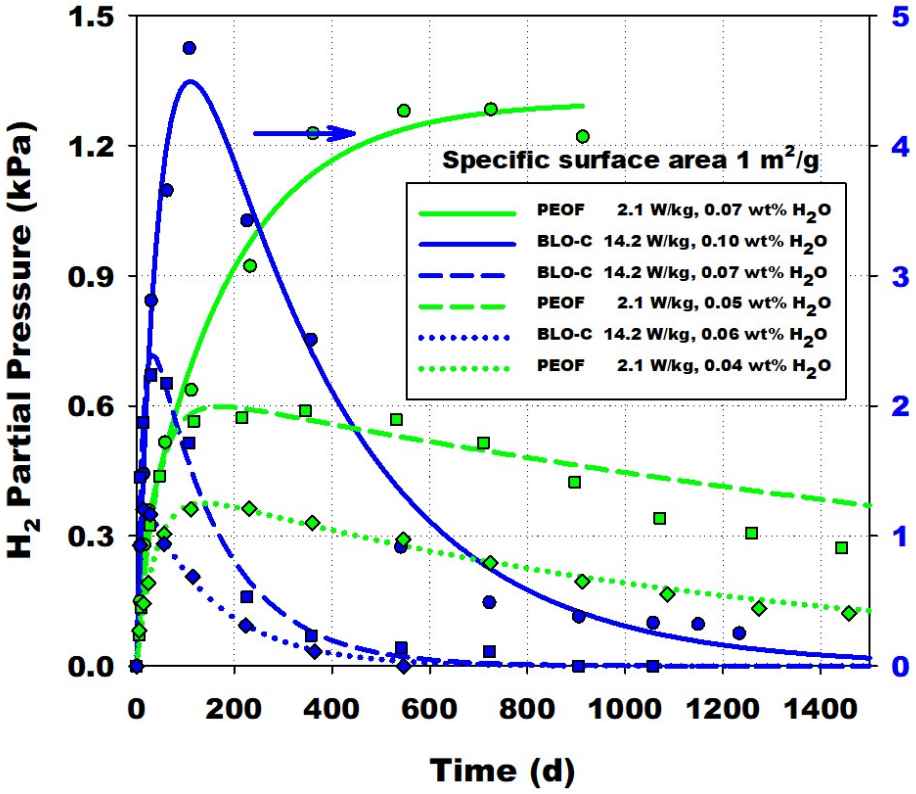

Figure 2. Hydrogen formation and consumption behavior of two high-purity oxides with similar specific surface area and different specific power.

The exposure of high-purity Pu oxides to air for long periods of time after stabilization affects their behavior when they are later placed in sealed containers. The effect of material aging is illustrated in Figure 3, which compares the partial pressure of hydrogen as a function of time for BLO and BLO-C. Both materials originated from MIS represented material BLO-39-11-004. The MIS represented material was calcined to 950 °C on June 19, 1997. Samples of this material were obtained in 2015 for RH studies. Both samples were calcined to clean the surface, exposed to 33% RH in a closed CHC for one week, and loaded into SSRs. However, the BLO sample was calcined to 400 °C, but the BLO-C sample was calcined to 950 °C. The BLO material aged in air for 18 years following its 950 °C calcination had a specific surface area approximately 6 times higher than that of the BLO-C material. As expected, the aged BLO material adsorbed about 6 times more water than the recently stabilized BLO-C material. The results of the experiments showed that the recently stabilized BLO-C material reached its maximum hydrogen

pressure and decreased to zero; whereas, the aged BLO material decreased to an equilibrium concentration of 8.5 kPa.

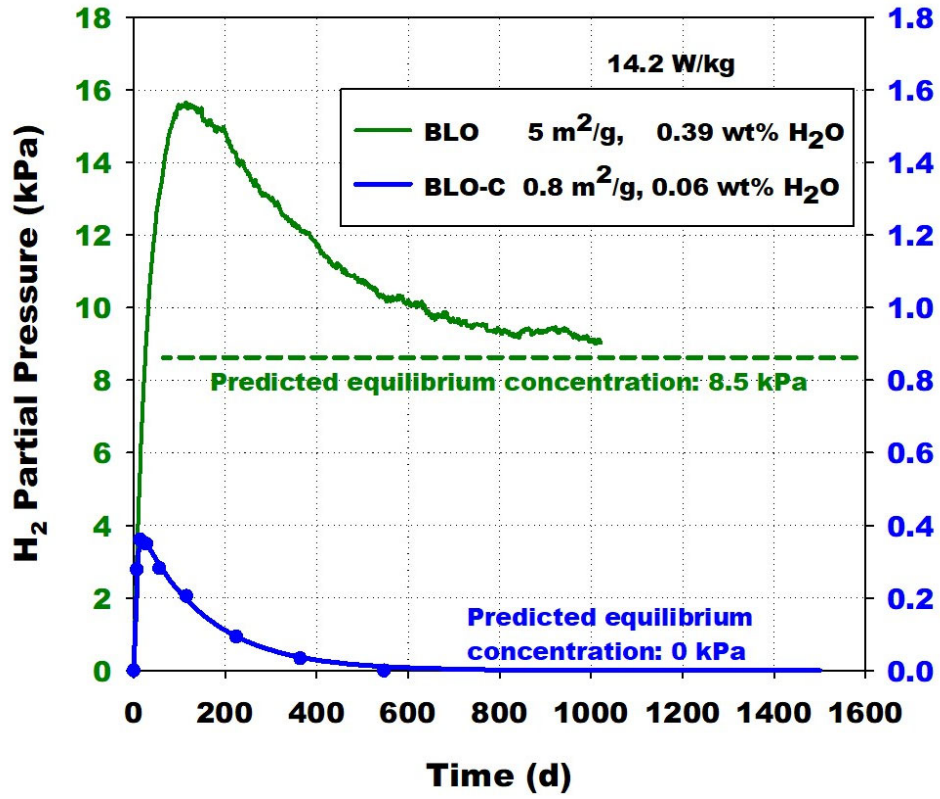

Figure 3. Hydrogen formation and consumption behavior of BLO and BLO-C. Both originated as samples of MIS Represented material BLO-39-11-004 calcined to 950 °C. BLO-C was calcined immediately before loading, but BLO was aged in air for 18 years prior to loading.

The formation and consumption of hydrogen and oxygen can be fit to first-order kinetic models. In the simplest case, water is radiolyzed to form hydrogen and consumption does not occur.

$$H_2O \xrightarrow{k_1} H_2$$

The pressure remains at its maximum indefinitely as shown in Figure 4. In this model, the fit parameter A_0 represents the initial active water in units of kPa, and the fit parameter k_1 is the rate constant representing the formation of the hydrogen with units of day^{-1}. The formation of hydrogen without consumption was shown to be incorrect because the maximum observed pressures in all experiments were less than 25% of the expected pressure resulting from complete radiolysis of the adsorbed water. A second model explained by the same curve includes rate constants for hydrogen formation (k_1) and consumption (k_2). In this case, the consumption is small relative to the initial active water A_0, and the active water can be considered a constant for long times. This model was also shown to be incorrect as the experiments progressed, because hydrogen was shown to decrease from its maximum, and the active water was found to decrease in all materials tested in the RH study. However, this model does explain the behavior of salt-bearing impure oxides described later in this report.

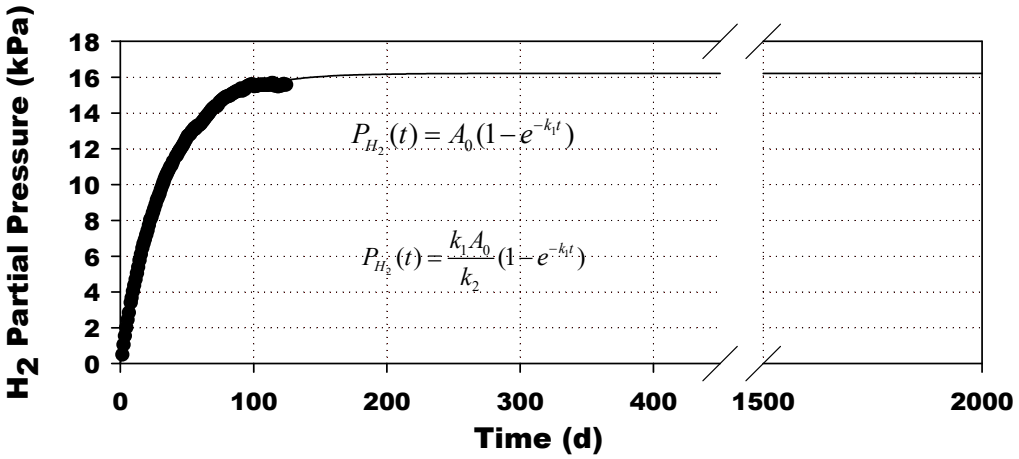

Figure 4. First order single parameter kinetic model for the formation of hydrogen without consumption. This model also explains the behavior of a first order two-parameter kinetic model in which the consumption is small with respect to the initial water.

Figure 5 shows a second model for hydrogen formation and consumption. In this model, hydrogen increases to a maximum, then eventually decreases to zero as it is consumed to form a species that does not re-form hydrogen.

$$H_2O \overset{k_1}{\rightarrow} H_2 \overset{k_2}{\rightarrow} solid\ adsorbate$$

In this case, consumption of the active water is significant, and the hydrogen pressure is not maintained indefinitely as in the previous model. This behavior is observed in high purity oxides that have been stabilized to 950 °C immediately before loading.

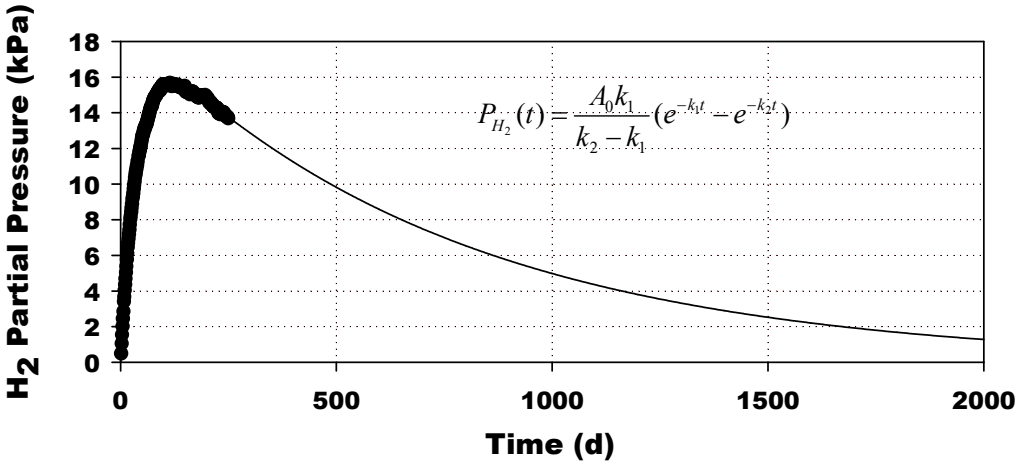

Figure 5. First order two-parameter kinetic model for the formation and consumption of hydrogen.

A third model for hydrogen formation and consumption in Figure 6 involves an equilibrium in which hydrogen increases to a maximum and is consumed to form a species that re-forms hydrogen.

$$H_2O \xrightarrow{k_1} H_2 \xrightleftarrows{k_2,-k_3} solid\ adsorbate.$$

The fit parameter k_3 is the rate constant representing the re-formation of the hydrogen. This behavior has been observed in high purity oxides that were calcined to 950 °C months to years prior to moisture addition and loading into the SSR. During the time between calcination and loading, the materials were aged in air. The specific surface area in these materials tends to be greater than 1 m^2 g^{-1} resulting in a larger capacity for moisture adsorption.

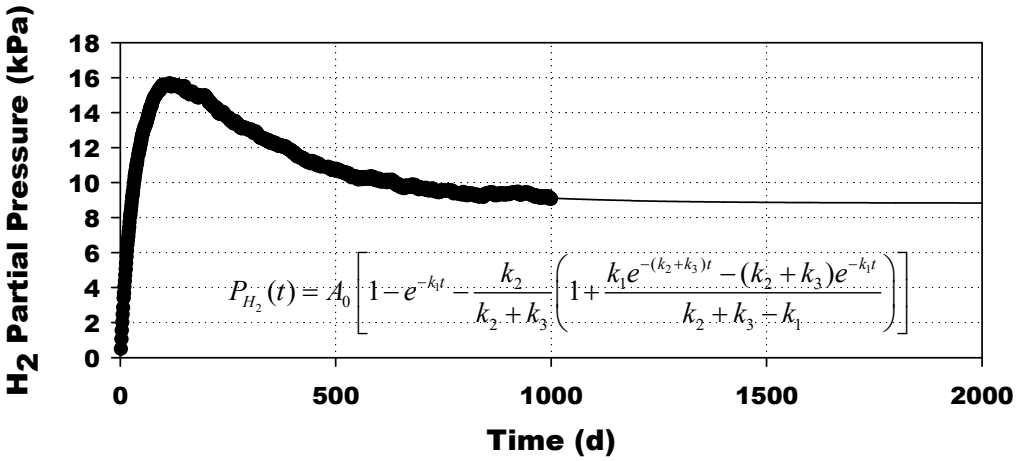

Figure 6. First order three-parameter kinetic model for the formation and consumption of hydrogen with equilibrium.

In all three models, the product of A_0 and k_1 gives the initial rate of hydrogen formation in units of kPa day^{-1}. These parameters can be used to calculate the hydrogen G value $G(H_2)$ according to Reference 30. For materials with the same specific power, the maximum hydrogen pressure is proportional to the initial rate of hydrogen formation and the amount of adsorbed water. Plotting the maximum hydrogen pressure as a function of the initial rate gives multiple straight lines with slopes that vary with the specific power. Normalizing the initial rate to the specific power places the points for all the materials on the same line as shown in Figure 7. Materials with an initial rate of hydrogen formation greater than 0.03 kPa day^{-1} W^{-1} also generate oxygen. The maximum oxygen pressure is also proportional to the initial rate of oxygen generation normalized to the specific power as shown in Figure 8.

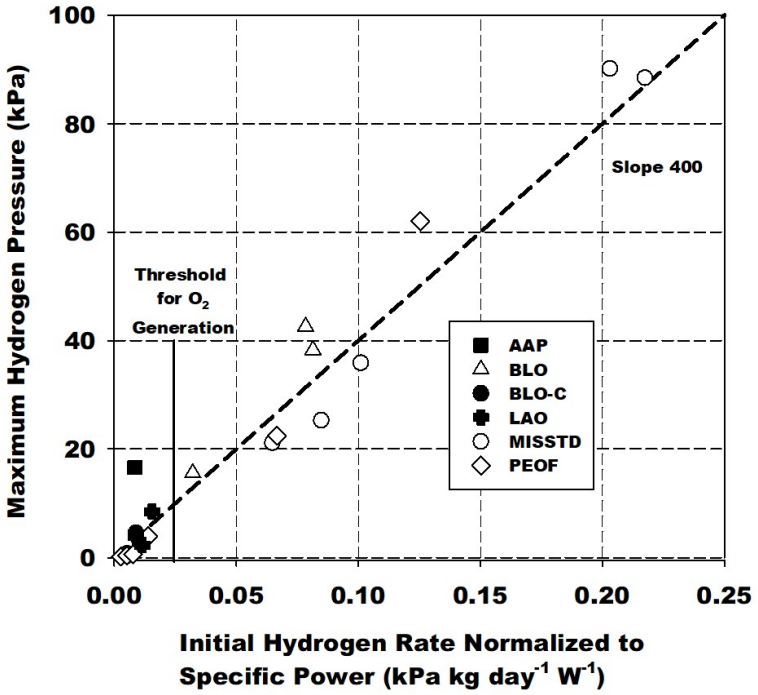

Figure 7. Maximum hydrogen pressure as a function of the initial rate normalized to the specific power for high-purity plutonium oxides equilibrated with a constant RH.

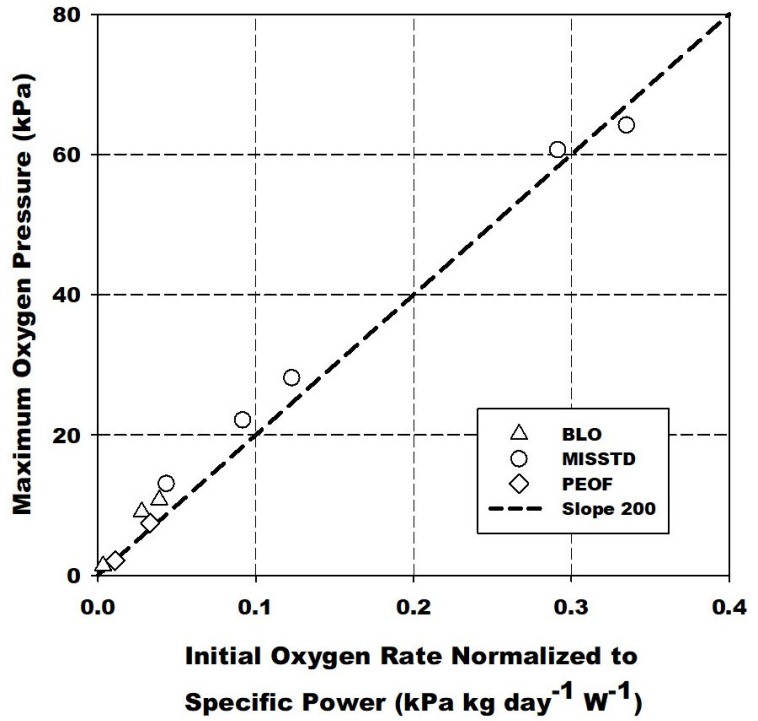

Figure 8. Maximum oxygen pressure as a function of the initial rate normalized to the specific power for high-purity plutonium oxides equilibrated with a constant RH.

Results

A comparison of the maximum pressures of the various gas species observed in the MIS Represented and RH study high-purity oxide shelf-life experiments is given in Table 2. For each of the materials, the table gives two temperatures in the calcination field. The first temperature is the original calcination temperature used when the material was processed by the MIS program (typically between 1997 and 2002), and the second temperature indicates the calcination temperature for the sample if calcination was performed again before loading (2003 and later). The table shows that the MIS represented high-purity oxides that were not calcined immediately before loading generated much higher amounts of carbon dioxide, nitrous oxide, and nitrogen than those that were calcined immediately before loading.

Table 2. List of High-Purity Oxides in Small-Scale Shelf-Life Experiments, Calcination Condition, Water Loading, and Maximum Pressures of Gas Species Observed.

Material	SSR	Experiment	Calcination	Water	$P_{max, H2}$	$P_{max, CO2}$	$P_{max, N2O}$	$P_{max, N2}$	$P_{max, CO}$
			Original / At Loading	(wt. %)	(kPa)	(kPa)	(kPa)	(kPa)	(kPa)
07161856	122†	MIS Rep.	950 °C / none‡	0.690	3.50	28.10	1.30	57.50	0.00
BLO-39-11-14-004	132A	MIS Rep.	950 °C / none	0.590	4.80	1.80	0.30	15.40	0.00
MT1490	125	MIS Rep.	950 °C / none	0.400	31.20	2.50	9.20	26.60	0.00
TS707001	123	MIS Rep.	950 °C / none	0.270	2.23	31.00	5.90	48.30	0.00
1000089	136‡	MIS Rep.	800 °C / none	0.650	16.8	0.00	1.7	31.2	0.00
ARF-102-85-114-1	154	MIS Rep.	950 °C / none	0.45	1.00	6.40	0.51	17.76	0.62
AAP02OX	251	RH Study	none / 400 °C	0.397	16.63	4.40	0.00	1.50	1.50
BLO-39-11-14-004	236	RH Study	950 °C / 400 °C	0.387	15.61	0.00	0.00	1.80	0.00
BLO-39-11-14-004	237	RH Study	950 °C / 400 °C	0.595	38.19	0.00	0.00	1.90	0.00
BLO-39-11-14-004	249	RH Study	950 °C / 400 °C	0.591	42.54	0.00	0.00	1.50	0.00
PEOF1	213	RH Study	950 °C / 400 °C	0.046	0.19	0.90	0.80	3.60	0.00
PEOF1	218	RH Study	950 °C / 400 °C	0.069	3.91	0.00	0.00	1.80	0.20
PEOF1	239	RH Study	950 °C / 400 °C	0.046	0.38	0.00	0.00	1.20	0.00
PEOF1	240A	RH Study	950 °C / 400 °C	0.054	0.60	0.00	0.00	1.80	0.00
PEOF1	242	RH Study	950 °C / 400 °C	0.265	22.47	0.00	0.00	1.80	0.00
PEOF1	243	RH Study	950 °C / 400 °C	1.066	61.98	0.90	0.00	1.60	1.00
MISSTD-1	244	RH Study	600 °C / 600 °C	1.049	21.15	0.00	0.00	2.30	0.00
MISSTD-1	245	RH Study	600 °C / 600 °C	1.193	25.28	0.00	0.00	2.60	0.00
MISSTD-1	246	RH Study	600 °C / 600 °C	1.338	35.87	0.00	0.00	2.40	0.00
MISSTD-1	247	RH Study	600 °C / 600 °C	1.824	88.43	0.00	0.70	3.70	0.00
MISSTD-1	248	RH Study	600 °C / 600 °C	1.800	90.15	0.00	0.50	3.60	0.38
LAO225BS	265B	RH Study	750 °C / 750 °C	0.273	2.28	0.00	0.00	1.60	0.00
LAO225BS	266A	RH Study	750 °C / 750 °C	0.387	3.87	0.00	0.00	1.70	0.00
LAO225BS	267A	RH Study	750 °C / 750 °C	0.534	8.50	0.00	0.00	2.10	0.00
BLO-39-11-14-004	256	RH Study	950 °C / 950 °C	0.058	0.36	0.00	0.00	0.00	0.00
BLO-39-11-14-004	257	RH Study	950 °C / 950 °C	0.074	0.72	0.00	0.00	0.00	0.00
BLO-39-11-14-004	258	RH Study	950 °C / 950 °C	0.104	4.49	0.00	0.00	0.00	0.00
MT1490	125A	MIS Rep.	950 °C / 950 °C	0.087	6.39	0.50	0.00	2.00	0.00
MT1490	125B	MIS Rep.	950 °C / 950 °C	0.063	4.90	0.00	0.00	0.00	0.00
1000089	136A	MIS Rep.	800 °C / 950 °C	0.100	10.50	0.00	0.00	1.50	0.00
PBO-47-09-012-023	142	MIS Rep.	none / 950 °C	0.500	5.50	0.00	0.00	4.30	0.00

†Sample SSR122 contained 13.7% unstabilized material.
‡Sample SSR136 contained 7.1% unstabilized material, 47.4% material calcined to 800 °C, and 45.6% material calcined to 950 °C.

Results

Many of the MIS represented high-purity Pu oxides loaded early in the shelf-life program were stopped and unloaded when the hydrogen reached its maximum value, so data showing the consumption of hydrogen was not collected. However, data collected for three materials in SSR132A, SSR123, and SSR154 (Figure 9) shows that the consumption behavior for materials aged in air prior to loading is characterized by the three-parameter model that includes a nonzero equilibrium pressure for hydrogen. This behavior is consistent with the behavior observed for aged materials in the RH study.

Two MIS Represented high-purity oxide samples generated flammable levels of oxygen. It was recognized after loading that SSR122, which was loaded with material 07167856 from the Rocky Flats peroxide precipitation process, contained 13.7% unstabilized material. The gas generation behavior of this material was dominated by nitrogen (57.5 kPa), oxygen (50 kPa), and carbon dioxide (28.1 kPa). A sample of 07161856 completely calcined to 950 °C was loaded into SSR122A and did not generate oxygen. Data collection are currently ongoing for this sample. Similar behavior was observed in SSR136 containing material 1000089 also from the Rocky Flats peroxide precipitation process. This sample contained 7.1% unstabilized material and the remainder was nearly a 50/50 mixture of materials calcined at 800 and 950 °C. A sample of 1000089 completely calcined to 950 °C was loaded into SSR136A and did not generate oxygen.

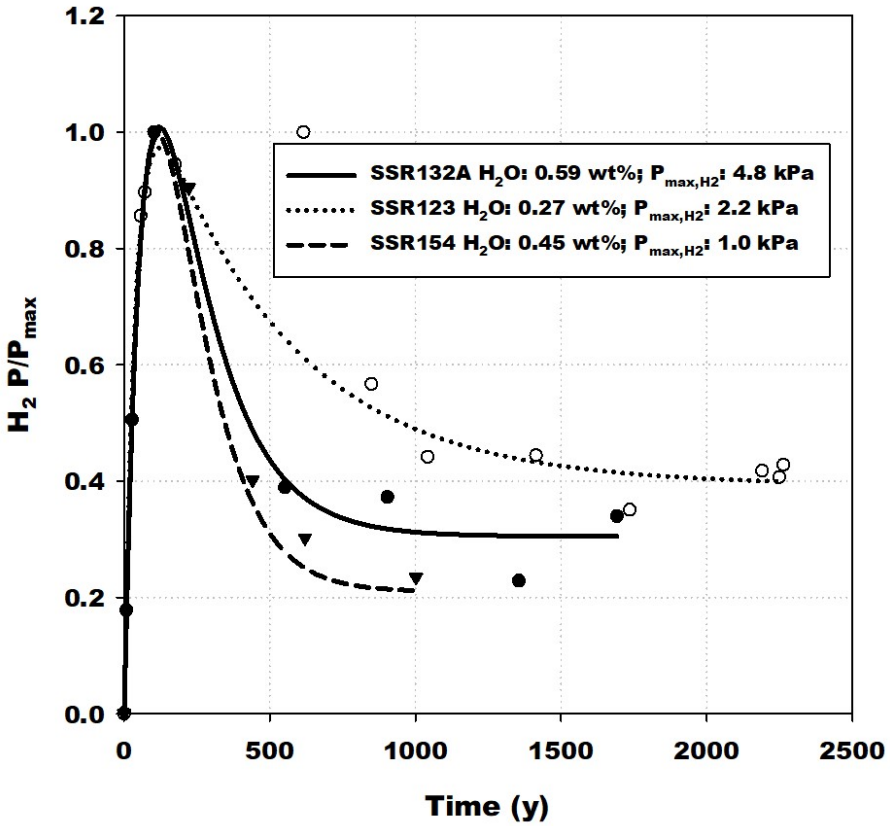

Figure 9. Hydrogen formation and consumption behavior observed in three MIS Represented high-purity oxide experiments allowed to continue after the hydrogen reached its maximum pressure.

3.1.1 *High Purity Mixed Pu-U Oxides*

The key observations from shelf-life experiments with high-purity mixed Pu-U oxides include the following:

1) The moisture adsorption behavior is influenced by the chemical form of the uranium in the material matrix.

2) The primary gas generation behavior of high purity mixed Pu-U oxides is described by models that include the formation and consumption of hydrogen produced by the radiolysis of water adsorbed on the oxide surface.

3) Oxygen was consumed in all experiments with the mixed Pu-U oxides.

4) The partial pressures of the other gases including carbon dioxide and nitrogen exceed the maximum hydrogen partial pressure in materials aged in air for months to years after calcination.

All the high-purity mixed Pu-U oxides were calcined months to years and aged in air prior to loading in the SSRs, and the gas generation behavior is dominated by the formation of carbon dioxide and nitrogen. The formation and consumption behavior of hydrogen is similar to the behavior of high-purity oxides; however, these materials may exhibit rapid moisture adsorption due to the formation of hydrated UO_3 rather than by surface adsorption.

The stoichiometry of the uranium oxide is important to understanding the experimental observations. The potential forms of uranium oxide are U_3O_8, UO_3, and UO_2. The stoichiometry U_3O_8 is formed from both UO_2 and UO_3 when uranium oxides are heated in air above 300 °C and 650 °C, respectively.[31] Calcination to 950 °C has the combined effect of converting the UO_2 to U_3O_8 and removing additional adsorbed species that were not removed in the 600 °C calcination. The formation of U_3O_8 through the reaction of UO_2 with oxygen results in a mass gain, whereas formation of U_3O_8 from UO_3 above 650 °C results in a mass loss. Following calcination at either 600 or 950 °C, U_3O_8 would be the predominant uranium species. Materials containing lower temperature stabilized material may have UO_3 present in the matrix.

The literature indicates that prolonged exposure of U_3O_8 to a high humidity environment has been shown to form UO_3.[32] The stoichiometry UO_3 is known to form hydrated compounds $UO_3{\cdot}xH_2O$ where $x = 0.5$, 0.8, 1.0, 2, and 2.25 when exposed to water vapor.[33] Therefore, the presence of UO_3 increases the capacity of high-purity mixed Pu-U oxides to adsorb water. Hydrated UO_3 is believed to be present in some MIS materials based on the TGA-MS and the moisture adsorption behavior.

The compound UO_3 undergoes a decomposition to U_3O_8 when heated above 650 °C.[31] The decomposition reaction results in a peak at 650 °C in the m/Z 32 (O_2) trace from the TGA-MS measurement. Figure 10 compares the m/Z 32 (O_2) traces for SSR126 and other high-purity mixed Pu-U oxides. The m/Z 32 (O_2) traces for SSR129 and SSR147 have large peaks at 650 °C and suggest that UO_3 was present. However, SSR126 and SSR135 do not show this same response at 650 °C, which suggests that these materials had very little UO_3 present and that the water observed from 200 to 500 °C was strongly bound water on the plutonium oxide surface.

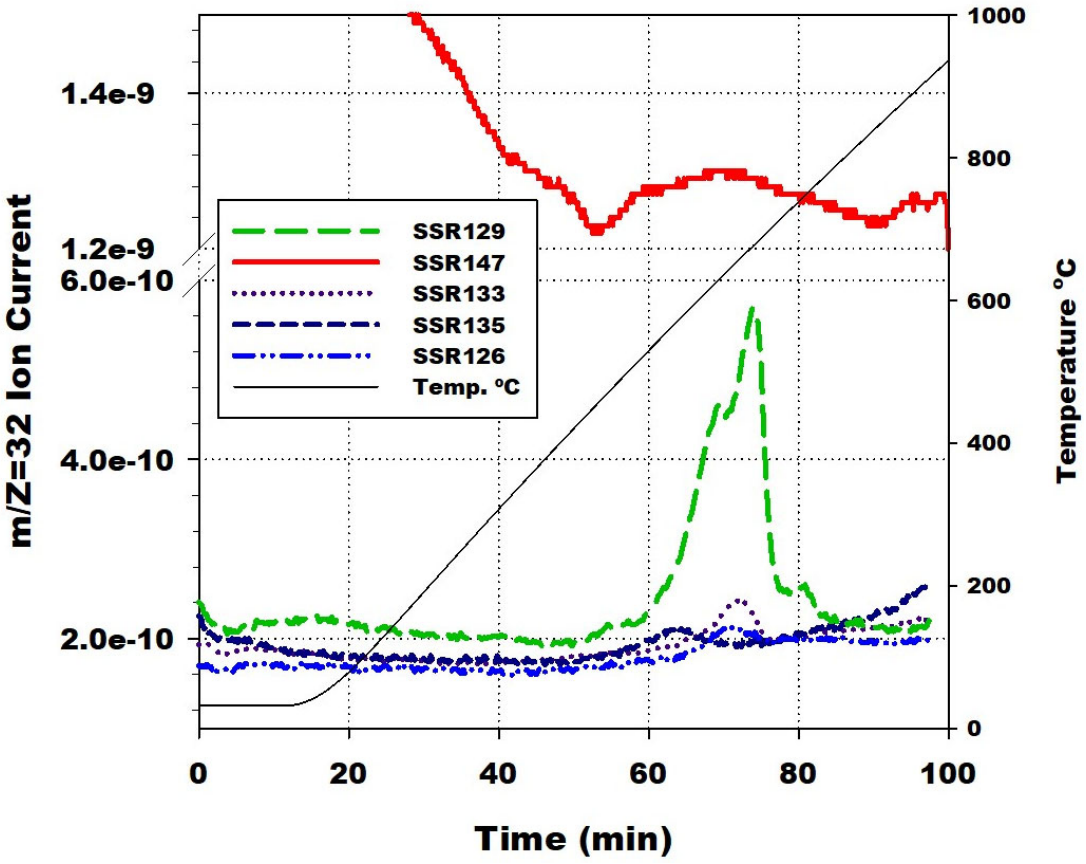

Figure 10. Comparison of the m/Z 32 (O_2) traces for high-purity mixed Pu-U oxides.

Figure 11 compares the moisture uptake for the same materials. Rapid moisture uptake is typically associated with the formation of hydrated salt compounds or in the case of high-purity mixed Pu-U oxides, hydrated UO_3 compounds. SSR126 and SSR135 have much slower rates of moisture uptake than SSR129, SSR133, and SSR147, which indicates surface adsorption rather than hydration of salts or UO_3.

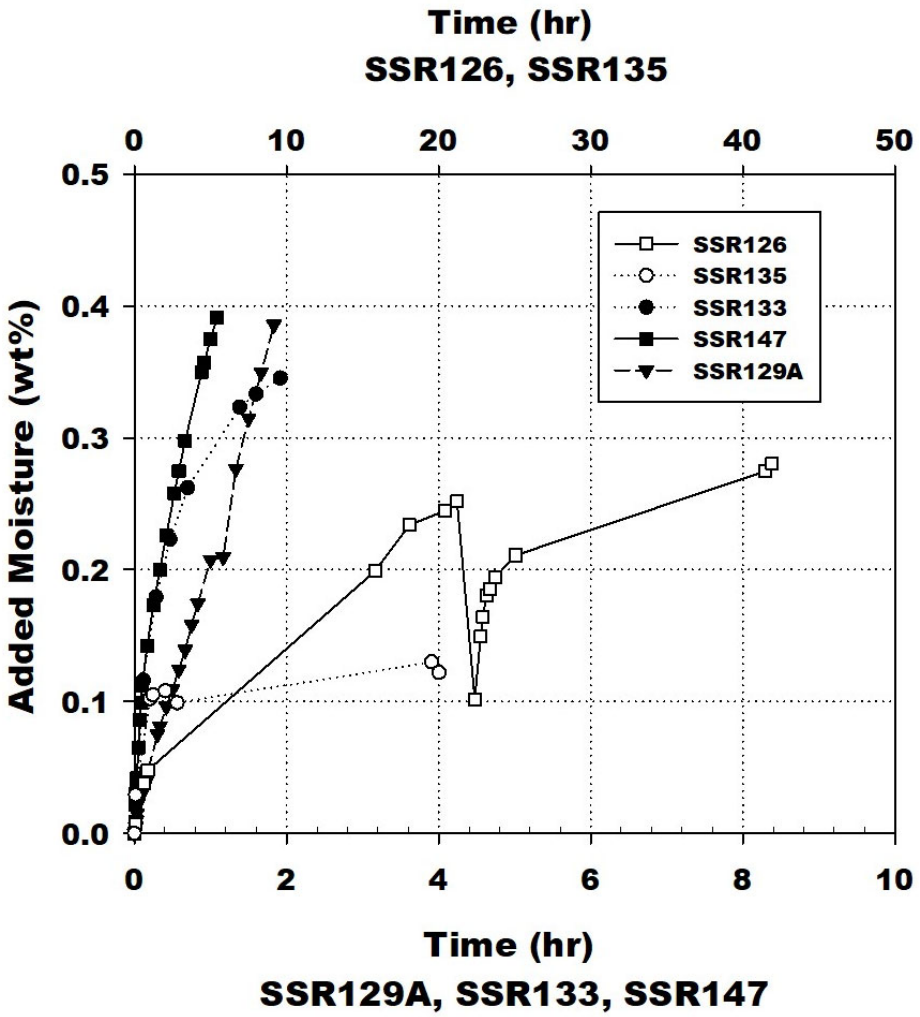

Figure 11. Comparison of moisture uptake data for high-purity mixed Pu-U oxides.

The hydrogen formation and consumption behavior of high-purity mixed Pu-U oxides is summarized in Figure 12 and Table 3. All the mixed Pu-U oxides were originally calcined to 950 °C months to years before loading. The gas generation behavior for most of the materials was dominated by carbon dioxide and nitrogen. In addition, all the mixed Pu-U oxides generated carbon monoxide, which was not observed in high-purity oxides without uranium. One sample was reloaded after calcining to 400 °C and had much lower carbon dioxide and nitrogen but still generated carbon monoxide. The hydrogen behavior for the two samples with higher amounts of UO_3 (SSR129 and SSR147) favor the three-parameter model with an equilibrium pressure for hydrogen; whereas the two samples where the UO_3 was converted to U_3O_8 (SSR126 and SSR135) tend toward zero after reaching the maximum pressure consistent with the two-parameter model.

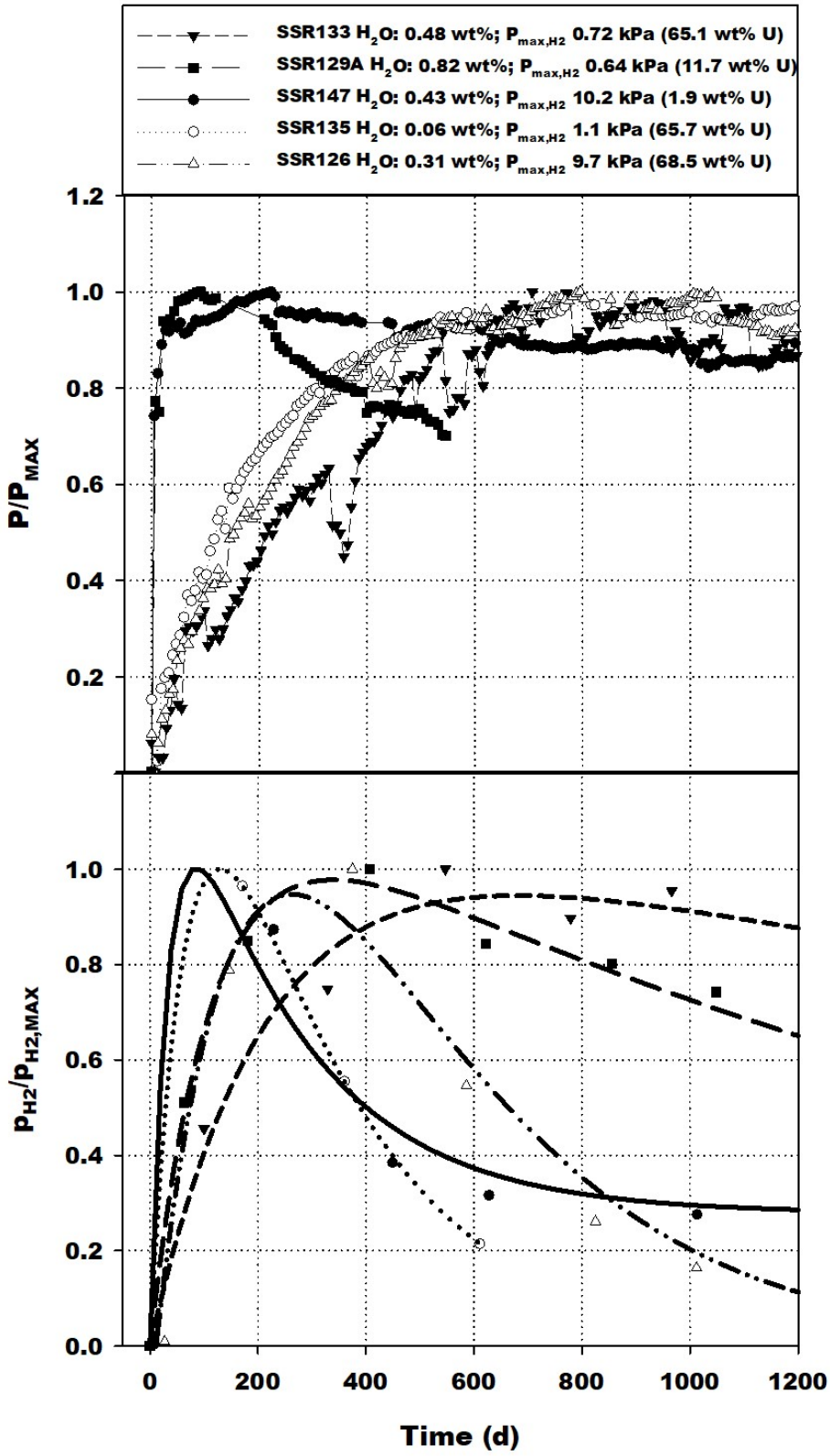

Figure 12. Normalized pressure curves and fits of the hydrogen formation and consumption behavior observed in MIS Represented high-purity mixed Pu-U oxide experiments.

Table 3. List of High-Purity Mixed Pu-U Oxides in Small-Scale Shelf-Life Experiments with Their Calcination Condition, Water Loading, and Maximum Pressures of Gas Species Observed.

Material	SSR	Calcination	Water	$P_{max, H2}$	$P_{max, CO2}$	$P_{max, N2O}$	$P_{max, N2}$	$P_{max, CO}$
		Original / At Loading	(wt. %)	(kPa)	(kPa)	(kPa)	(kPa)	(kPa)
5501579	124	950 °C / none	0.330	1.16	29.10	5.70	48.00	6.20
5501579	124A	950 °C / 400 °C	0.230	5.70	2.40	0.10	1.00	2.40
669194	126	950 °C / none	0.310	9.52	12.80	0.90	6.30	3.70
PSU-84-06-05	133	950 °C / none	0.470	0.72	3.2	1.77	15.00	2.02
5501407	129	950 °C / none	0.820	0.73	17.70	2.00	55.50	0.57
SCP711-46	135	950 °C / none	0.060	1.00	29.80	1.50	8.30	6.70
CAN92	147	950 °C / none	0.430	10.50	6.30	2.30	24.80	1.60

3.2 Salt-Bearing Impure Oxides

The key observations from shelf-life experiments with salt-bearing impure Pu oxides include the following:

1) Moisture adsorption behavior depends on the chemical form of the chloride salts in the material matrix.

2) The gas generation behavior of salt-bearing impure oxides is dominated by the formation of hydrogen. The partial pressure of hydrogen reaches a maximum where it remains for many years until finally decreasing.

3) Oxygen generation has been observed and is associated with liquid phase formation in the material. Flammable conditions can occur and persist for years, but the oxygen eventually decreases below flammability at long times.

The water in salt-bearing impure oxides is held by alkaline earth chlorides, mainly $CaCl_2$ with some $MgCl_2$ that survived the calcination. The RH inside the container is controlled by the hydrated salt mixture. The alkaline earth chlorides form hydrates at low RH and deliquesced liquids at higher RH, above 30%. Radiolysis of hydrated salts forms hydrogen and HCl. Radiolysis of deliquesced liquids form hydrogen, HCl and Cl_2. In high-purity oxides the water is a physisorbed layer on the oxide surface and radiolysis is thought to be more similar to liquid water. At high RH, the number of monolayers of physisorbed water are high, and the $G(H_2)$ approaches that of liquid water. Thus, the radiolysis mechanisms are different for the two types of materials. Nevertheless, the trends over time are similar.

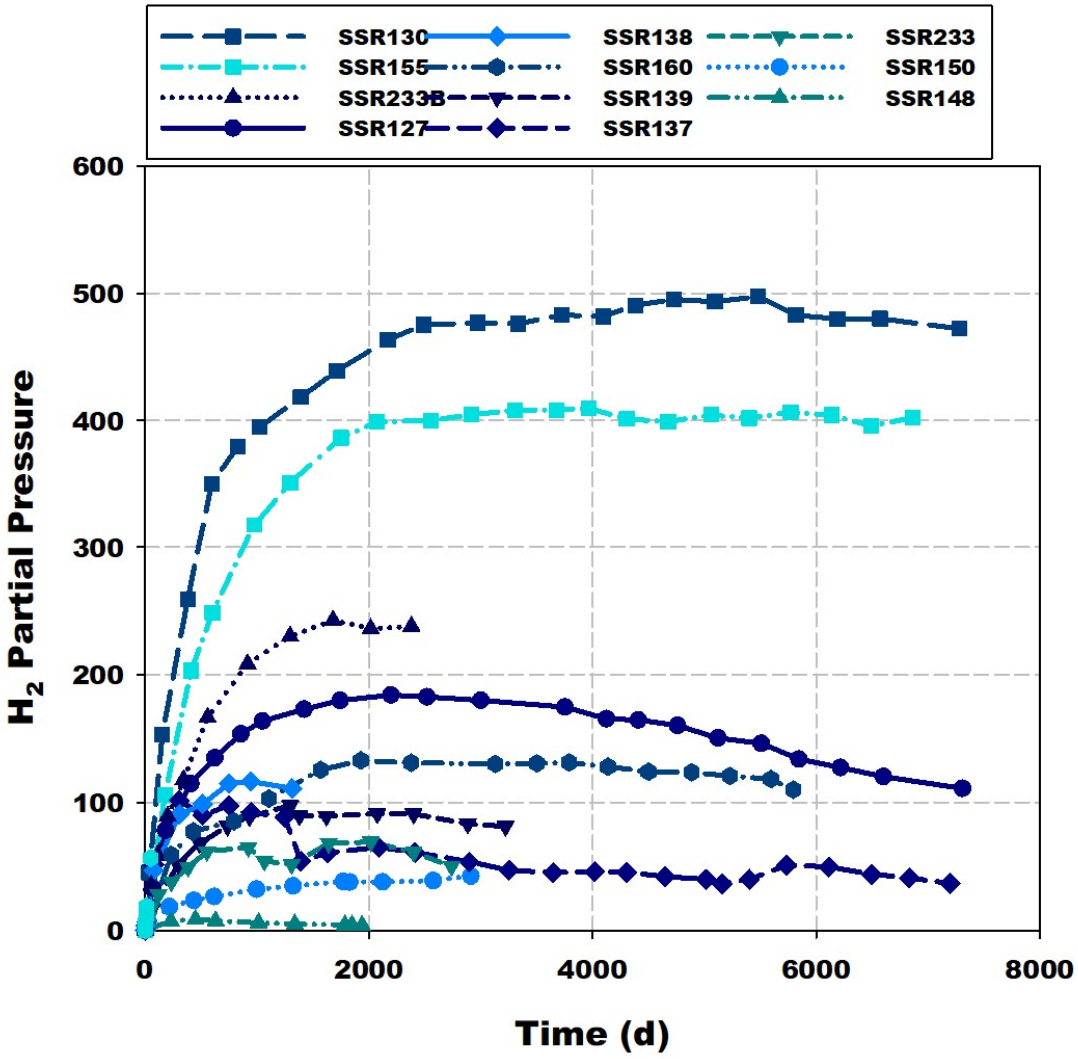

Figure 13 Partial pressures of hydrogen as a function of time for eleven salt-bearing impure Pu oxides loaded with approximately 0.5 wt. % water then sealed and loaded in SSRs.

The hydrogen gas generation behavior of salt-bearing materials has some of the same characteristics of high-purity oxides. As shown in Figure 13, the behavior is characterized by a high initial rate of hydrogen formation, a gradual slowing of the hydrogen pressure increase, a plateau region, and eventually a decline in hydrogen pressure. The maximum hydrogen pressure is generally higher than the maximum pressure in high-purity oxides and can be one to two orders of magnitude higher for the same fraction of adsorbed water. The plateau lasts longer, and for some salt-bearing materials, the start of the decline in the hydrogen pressure occurs at fifteen years or later.

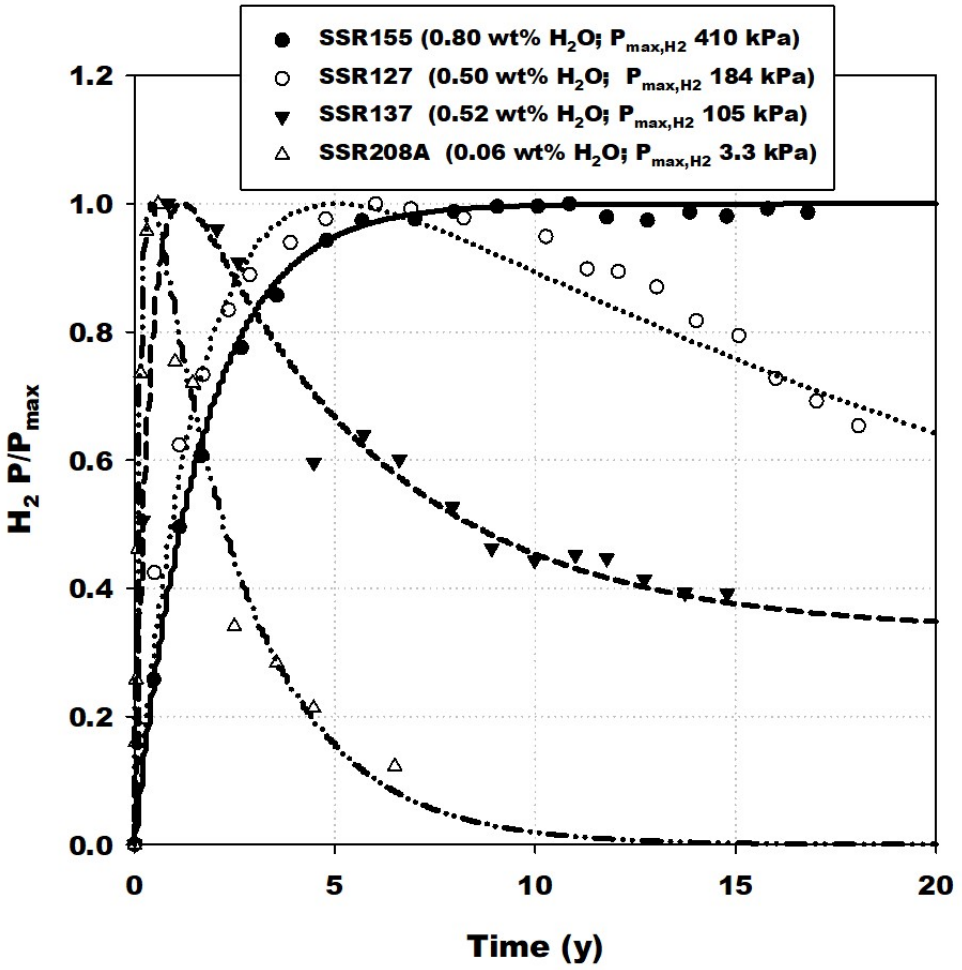

Figure 14. Hydrogen formation and consumption behavior observed in MIS Represented salt-bearing impure Pu oxides.

A plot of the normalized hydrogen pressures shown in Figure 14 illustrates some typical behavior for salt-bearing materials. Calcination just prior to loading results in a longer plateau at the maximum pressure (SSR127 and SSR155). Calcination followed by aging for years prior to loading (SSR137 and SSR208A) results in reaching the maximum hydrogen pressure in shorter times, one to two years. SSR137 fits the model where hydrogen is re-formed from a surface species, which results in a long-term hydrogen partial pressure. SSR208A has a low chloride content of 1.2% and reaches a maximum hydrogen pressure of 3.3 kPa. As the amount of water increases, the amount of time required to consume the water also increases.

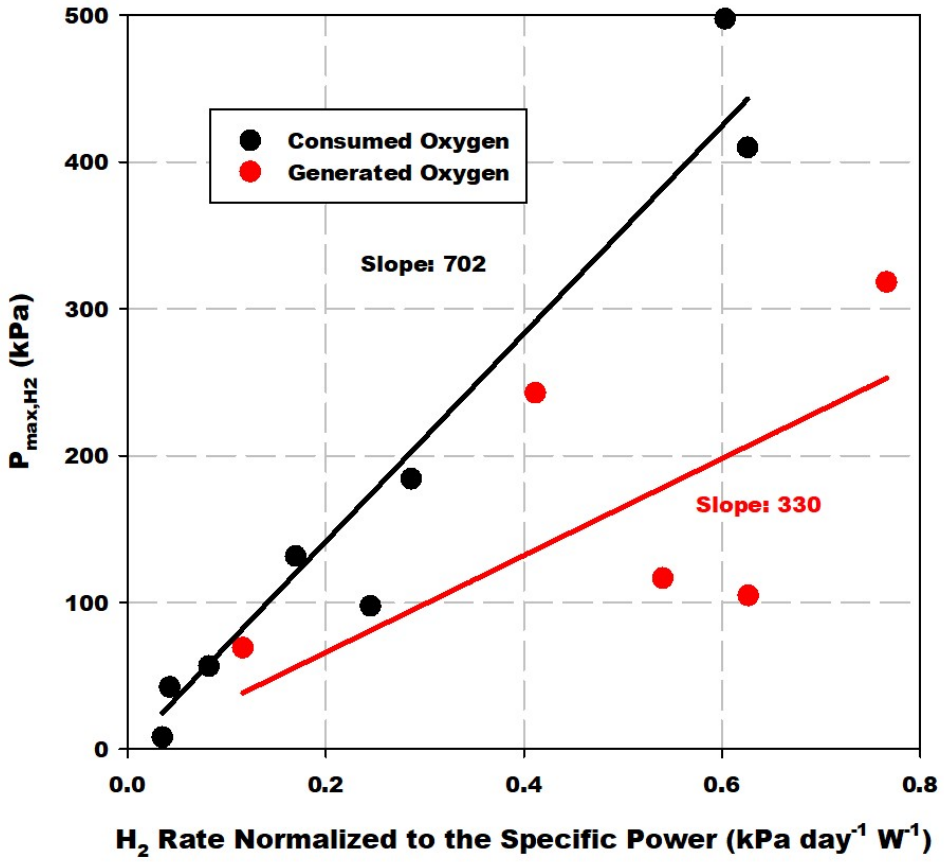

Figure 15. Maximum hydrogen pressure generated by MIS Represented salt-bearing impure Pu oxides as a function of the initial rate normalized to the specific power for the material.

The maximum hydrogen pressure plotted as a function of the hydrogen gas generation rate normalized to the specific power (Figure 15) increases linearly as seen with high-purity Pu oxides. It appears that materials that generate oxygen have a lower slope than materials that do not generate oxygen. The salt-bearing materials that do not generate oxygen have a slope that is 75% higher than that of high-purity oxides. The materials that generate oxygen contain deliquesced liquids. The slope for the maximum hydrogen pressure with deliquesced liquids is half that of salt-bearing materials with hydrated alkaline earth chlorides. A plausible explanation for this effect is that the mechanism to produce hydrogen for a brine is fundamentally different than the mechanism for the production of hydrogen from a hydrated salt. There is no threshold for oxygen generation. In salt-bearing impure oxides, the amount of water needed to form a deliquesced liquid is a function of the amount of alkaline earth chlorides and, therefore, the hydrogen generation rate and maximum hydrogen pressure varies with the amount of alkaline earth chlorides. For instance, low amounts of alkaline earth chlorides can result in deliquesced liquids at a low water content; therefore, these materials have a low hydrogen generation rate and low maximum pressure of hydrogen. Materials with high concentrations of alkaline earth chlorides require higher moisture content for deliquescence; therefore, these materials have higher hydrogen generation rates, higher maximum pressures, and show the consumption of oxygen.

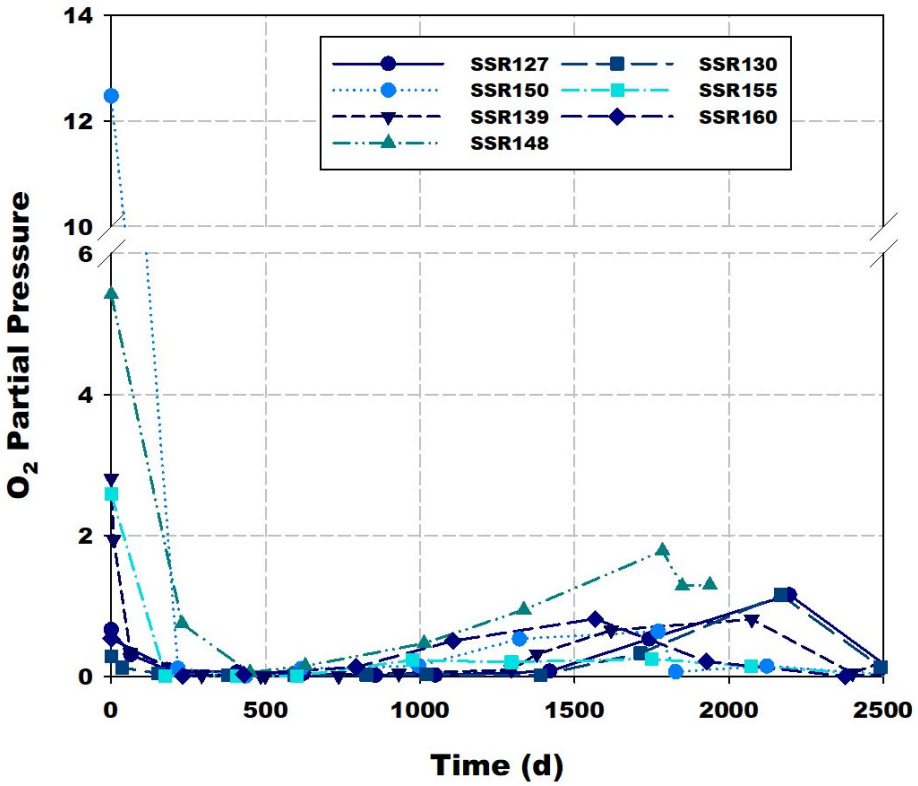

Figure 16. Behavior of oxygen in MIS Represented salt-bearing impure Pu oxides in which oxygen was initially consumed.

Figure 16 shows the oxygen consumption behavior for the salt-bearing impure Pu oxides where liquid phases did not form. In these materials, the oxygen falls to zero within a few hundred days. However, at long times, increases in the partial pressures of oxygen of up to two kPa were observed in many of these materials after about four years. A review of the gas composition data for these materials shows that the gas samples with higher oxygen partial pressures all occurred on the same sampling dates between October 2007 and November 2010. These gas samples also showed corresponding increases in the nitrogen partial pressure. These results indicate that the increase in the oxygen partial pressure observed for these samples was due to an air leak into the gas sampling manifold rather than the generation of oxygen by the material.

For salt-bearing impure oxides that do generate oxygen, the oxygen peaks and then falls, usually to zero as shown in Figure 17. A favorable ratio of the alkaline earth chlorides and moisture can result in the oxygen partial pressure remaining elevated for years as seen in SSR137. This material had approximately 0.6 wt. % alkaline earth chloride and 0.5 wt. % moisture and is shown by the star in Figure 18. The increases in oxygen seen at ~1200 days and ~5200 days are due to temperature excursions to 200 °C due to heater controller failure. After each temperature excursion the oxygen partial pressure returned to values consistent with a fit of data prior to the excursion. This return took approximately two years. Oxygen partial pressures of 30 to 40 kPa that are seen in these materials result in a flammable gas mixture for a window of time before the oxygen partial pressure drops sufficiently for the gas mixture to become non-flammable. The hydrogen partial pressure remains higher than the oxygen partial pressure at long times; therefore, at long times it is the oxygen behavior that determines when flammability ceases.

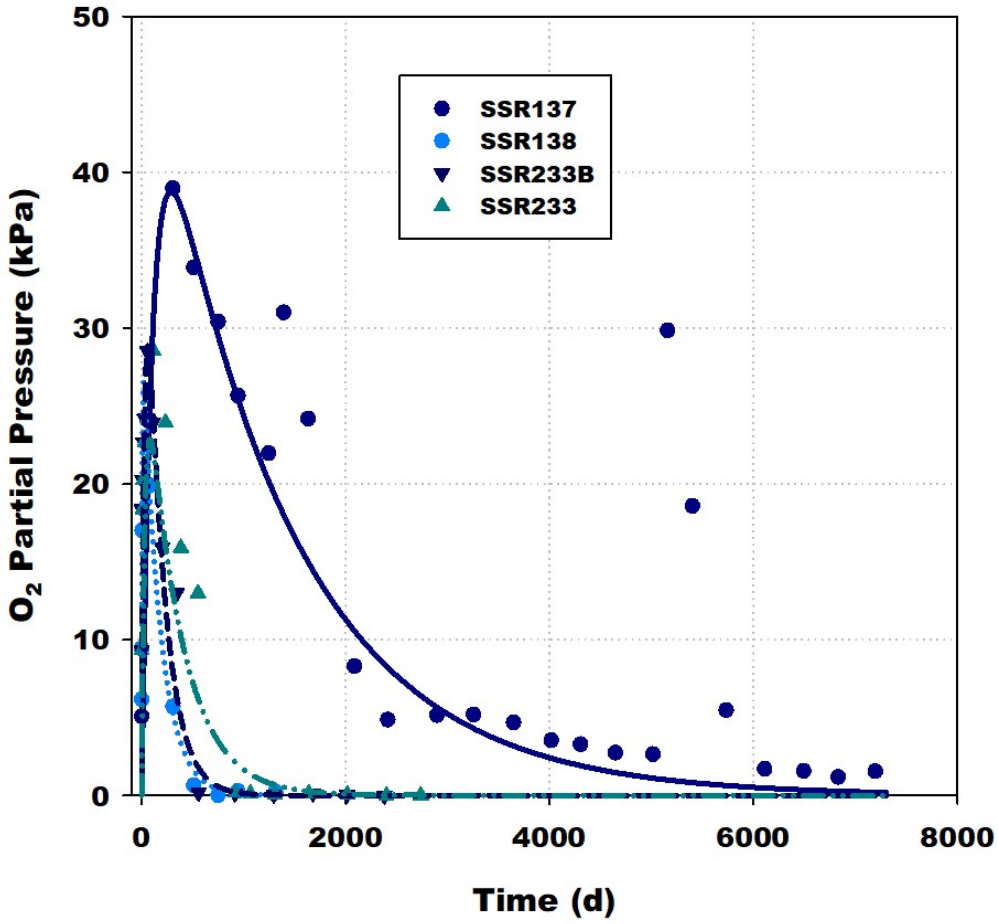

Figure 17. Oxygen formation and consumption behavior observed in MIS Represented salt-bearing impure Pu oxides that generated oxygen.

Oxygen generation occurs in salt-bearing impure oxides when liquid phases are present in the material. Liquid phases form above two waters of hydration in calcium chlorides and above six waters of hydration in magnesium chlorides. Conditions for oxygen generation in salt-bearing impure oxides are shown in Figure 18. The region with the potential for flammable mixtures of hydrogen and oxygen is bounded by materials having 0.25 wt.% water and two to seven waters of hydration adsorbed onto the alkaline earth chloride salt. A region was previously identified based on a set of experiments that reproduced the salt composition of 011589A material, a MIS represented sample that generated a flammable mixture of hydrogen and oxygen gases.[34] It was originally reported that the conditions for oxygen generation required a moisture content of 0.3 wt. % or higher and alkaline earth chloride salt with waters of hydration between three and seven. More recent data from small- and large-scale experiments have shown flammable mixtures of hydrogen and oxygen in other salt-bearing materials. Some materials fall outside of this region, but the uncertainty in the amount of alkaline earth chloride present may affect the position of those experiments on the plot. For example, the Large-Scale Corrosion Series II test containers had added salt that was not calcined with the material and have uneven distribution of water on the salt, which was evident based on the uneven corrosion observed on the inside of the container body.[35] In the case of the H003328 samples, some of the alkaline earth chloride in the material may have been destroyed by the radiolytic consumption of the chloride salt after it was packaged in its original container.[36] This would move the lowest flammable point up and to the left towards the original region with the lower bound of

0.3 wt. % moisture and 3 to 7 waters of hydration on the alkaline earth chloride salt. This is supported by evidence that the H003328 material caused gas phase corrosion of the original inner 3013 but no longer generates chloride containing gases in recent experiments.[37]

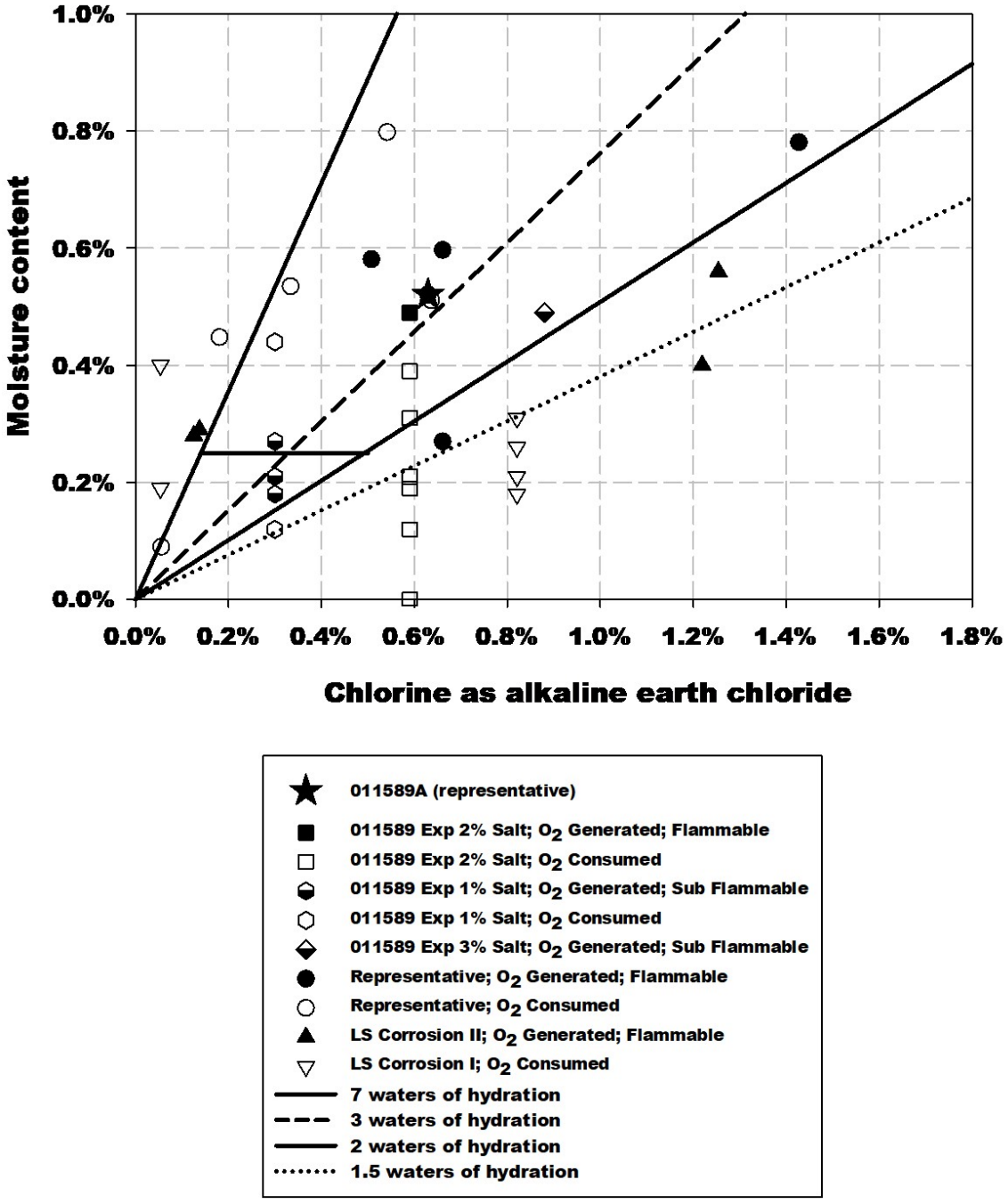

Figure 18. Salt-bearing impure oxide moisture content plotted as a function of the weight percent chlorine in the form of alkaline earth chloride. Salt-bearing impure oxides generate oxygen when liquid water is present. Calcium chloride deliquesces above two waters of hydration which forms the lower bound for oxygen generation as the chloride concentration increases. At low salt content and high moisture, dilute salt solutions may form. These don't form oxygen.

3.3 Comparisons of High-Purity and Salt-Bearing Impure Oxides

The hydrogen pressure as a function of time in sealed containers for all materials studied shows an initial rise followed by a maximum pressure and eventually a decrease in pressure. The principal differences between high-purity oxides and materials with salts are (1) the initial rates normalized by the specific power can achieve higher values for the salt-bearing impure oxides that do not generate oxygen, and (2) the plateau following the maximum pressure lasts longer for the salts. The higher initial hydrogen gas generation rate for some salts arises from a higher $G(H_2)$.

The $G(H_2)$ can be calculated from the initial rate of hydrogen formation, the water content, and the dose to the water.[30] The dose to water is calculated using the stopping power of all impurities. The value for alpha radiation of liquid water is 1.3 molecules per 100 eV (0.13 micromoles J^{-1}; 130 nanomoles s^{-1} W^{-1}) and is indicated as the blue line in Figure 19 and Figure 20. For the high-purity oxides, a range of $G(H_2)$ is calculated from ~0.02 to 0.4 molecules per 100 eV of adsorbed dose (0.002 to 0.04 micromole per J; 2 to 40 nanomole s^{-1} W^{-1}). Figure 19 shows that there is no dependence on the plutonium oxide surface water coverage (as expressed in monolayers of water) in the range studied, and the $G(H_2)$ values are all below that of liquid water.

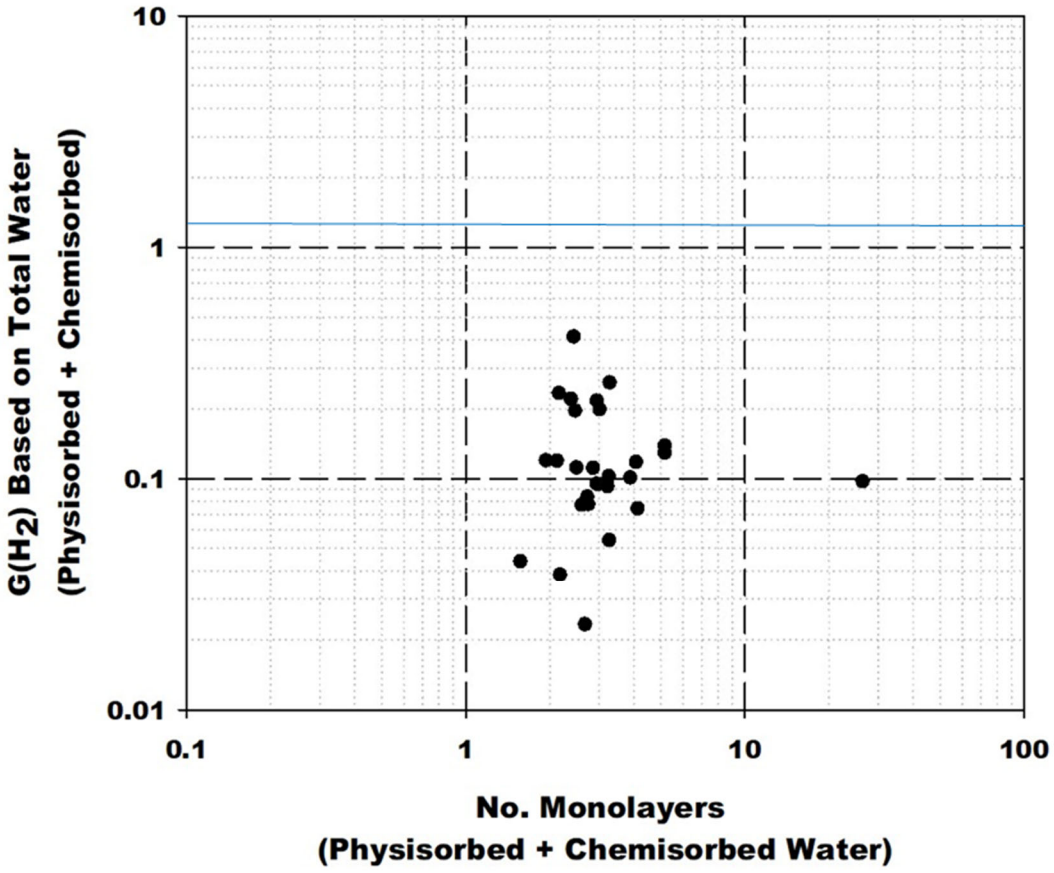

Figure 19. Hydrogen G-values calculated for high-purity Pu oxides as a function of monolayers of adsorbed water.

The behavior of $G(H_2)$ for salt-bearing materials is similar to that of high-purity oxides. There is a similar range over a factor of 20 from 0.2 to 5 molecules per 100 eV (0.02 to 0.5 micromole J^{-1}; 20 to 500 nanomoles s^{-1} W^{-1}) with the absolute values being approximately an order of magnitude higher. This ignores the outlier at 0.04. The water in salt-bearing materials is primarily found in association with alkaline earth chlorides, which form hydrates or, if the RH is sufficiently high, deliquesced liquids. Figure 20 shows that here is no trend in $G(H_2)$ with the number of waters associated with the alkaline earth chlorides.

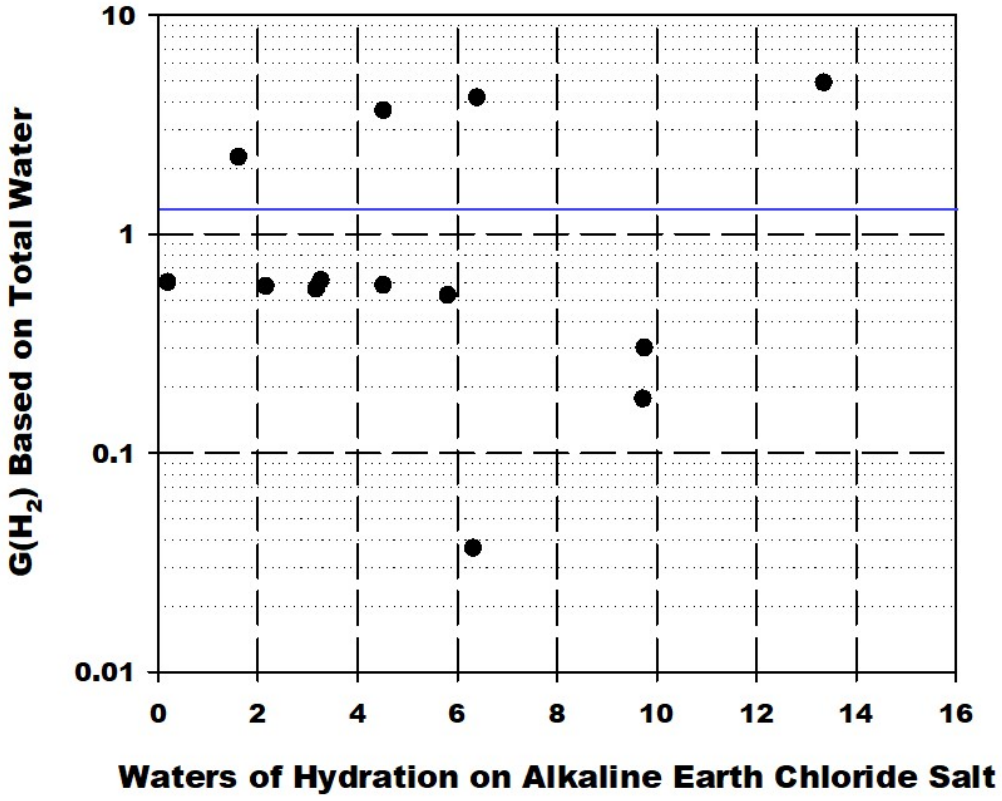

Figure 20. Hydrogen G-values calculated for salt-bearing impure Pu oxides as a function of the numbers of waters of hydration of the alkaline earth chlorides.

3.4 Comparison between Small-Scale Reactors and Large-Scale Containers

There are a few comparisons between the hydrogen gas-generation behavior observed in the SSRs and the large-scale containers where the same material was used and the amount of added water was similar in both experiments. To compare the hydrogen gas pressure, the SSR pressure is scaled by both the amount of water and the ratio of the free gas volume in the large-scale compared to the small-scale. In the case of high-purity oxides, small- and large-scale experiments with PEOF are compared in Figure 21. This material has a low specific surface area, ~1 m^2 g^{-1}, and a relatively low specific power, 2 W kg^{-1}. The hydrogen pressure rises to a maximum of 0.35 to 0.45 kPa in 200 days and then starts to decrease in both systems. Similar to the small-scale experiment, the large-scale PEOF material did not generate carbon dioxide or nitrous oxide and had between 1 and 2 kPa of nitrogen present.

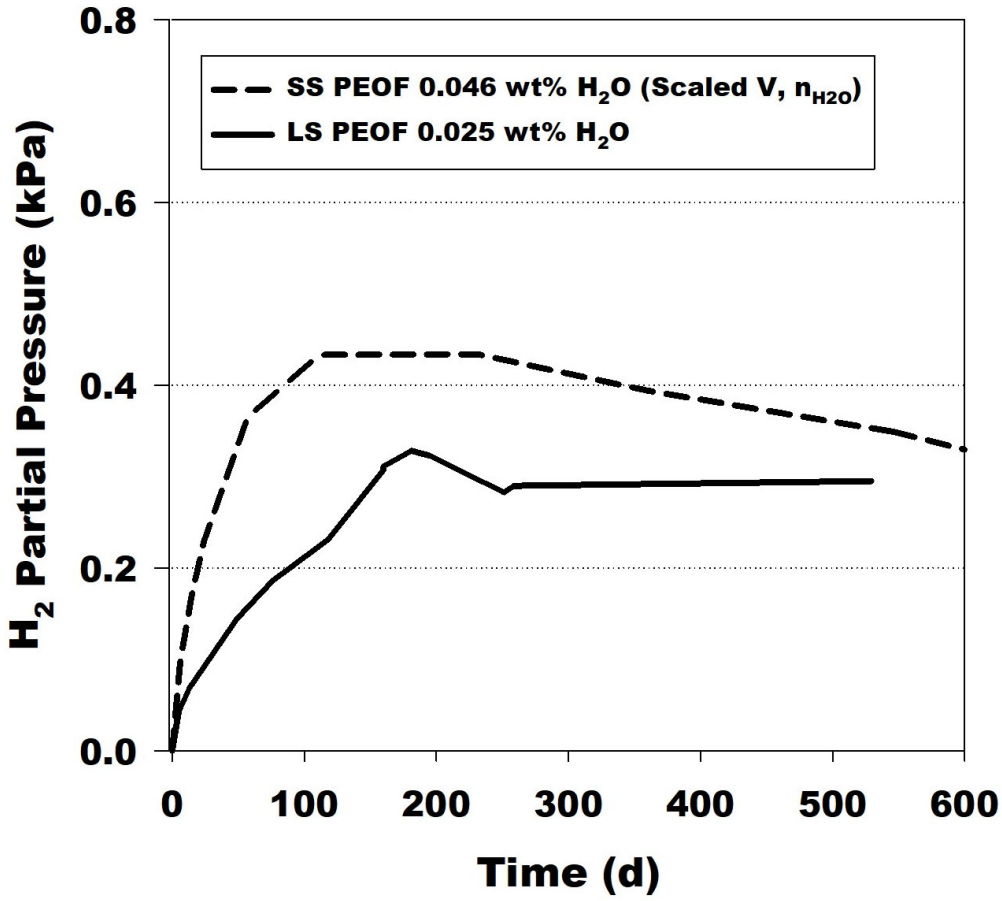

Figure 21. Comparison of the hydrogen gas formation and consumption behavior for high-purity oxide PEOF in a SSR and a large-scale container. The SSR data is scaled by both the free-gas volume and moles of water to be equivalent to the conditions in the large-scale container.

To compare the hydrogen gas generation of a salt-bearing material between systems, the material PMAXBS was chosen. This material has 71% plutonium and a specific power of 1.7 W kg^{-1}. In this case, the SSR results were scaled by both the moles of water and the ratio of the free gas volumes. As shown in Figure 22, the pressure in both systems rose to approximately 60 kPa in 2,000 days and then began to decline. These data show that the results from experiments in SSRs can be used to predict the behavior of hydrogen gas generation in 3013 containers if the free-gas volume and amount of water is known. Other gases including nitrogen, carbon dioxide, carbon monoxide, and methane were observed in the small-scale experiment, which increased the total pressure approximately 30 kPa. These gases were observed in only trace amounts in the large-scale experiment. These differences may be explained by the material handling and the time between stabilization and loading the material.

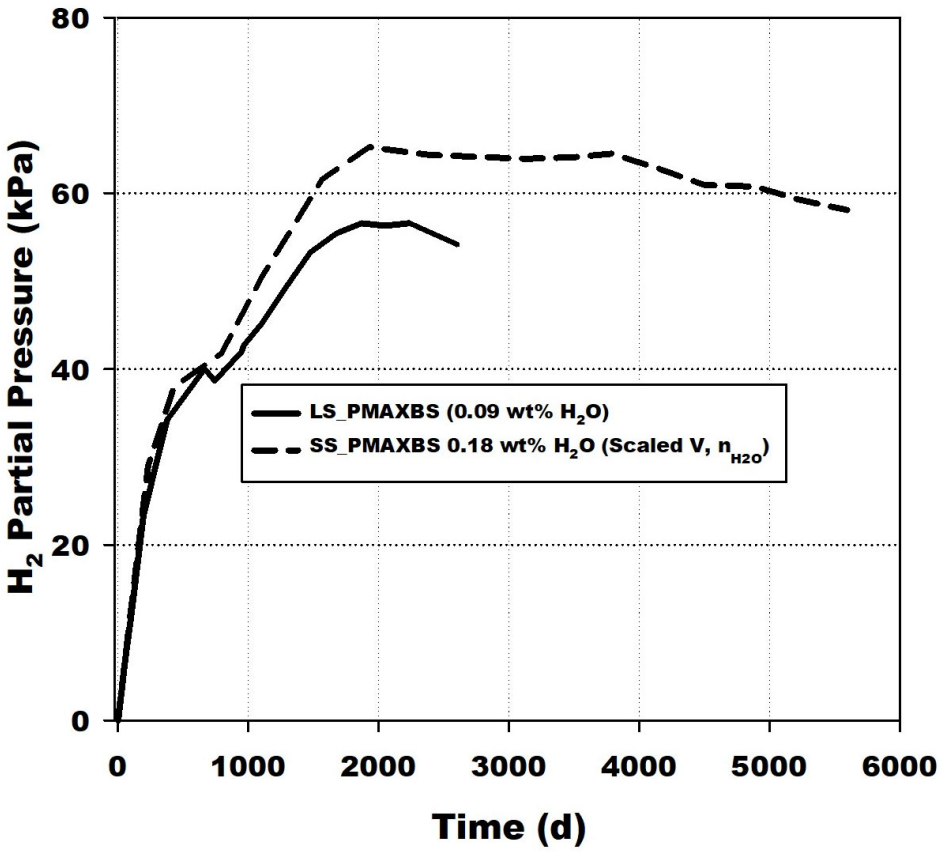

Figure 22. Comparison of the hydrogen gas formation and consumption behavior for salt-bearing impure oxide PMAXBS in a SSR and a large-scale container. The SSR data is scaled by both the free-gas volume and moles of water to be equivalent to the conditions in the large-scale container.

A direct comparison between an actual 3013 and a small-scale test was done using the material that was originally packaged in 3013 container H003328 from Hanford.[38] A discrepancy in the TGA results for the stabilized material at the time of packaging resulted in the potential for this container to have closed with material slightly in excess of the moisture content allowed by the 3013 Standard. The container was shipped to LANL, and a gas sample was obtained using the can puncture device. The pressure of the inner container was found to be 43.4 psia.[39] A GC analysis of the gas within the inner container determined the composition to be 14.2% helium, 11.3% nitrogen, and 74.4% hydrogen. No oxygen or other gases were detected.

Samples of the material removed from the container were loaded into SSRs. One sample SSR233 was loaded in its as-received condition without adding or removing water. A second sample SSR234 was dried by heating to 200 °C to remove the 0.27 wt.% water remaining on the material at the time the material was unloaded from the inner 3013 container. The moisture content was then increased to the original 0.53 wt.% using the humidified balance. A third sample SSR233B was loaded after adding water to the as received material to bring the moisture content from 0.27 wt.% to the original 0.53 wt. %. A fourth sample SSR233A was loaded under the same conditions as the third sample but was removed after one month due to a leak.

Results

The hydrogen and oxygen partial pressures from the three small-scale experiments with H003328 material are shown in Figure 23. All three samples generated flammable mixtures of hydrogen and oxygen, but the gas mixture was no longer flammable after two years. (SSR233 experienced a temperature excursion, which affected the gas composition between 900 and 1,500 days). The two samples with nominally 0.5 wt. % water have similar hydrogen pressures. The "X" on the plot indicates the hydrogen and oxygen partial pressures of the actual 3013 at the time it was opened. Fits obtained of the SSR233B data indicate that the hydrogen partial pressure will be the same as or very close to the actual 3013 container when it was opened.

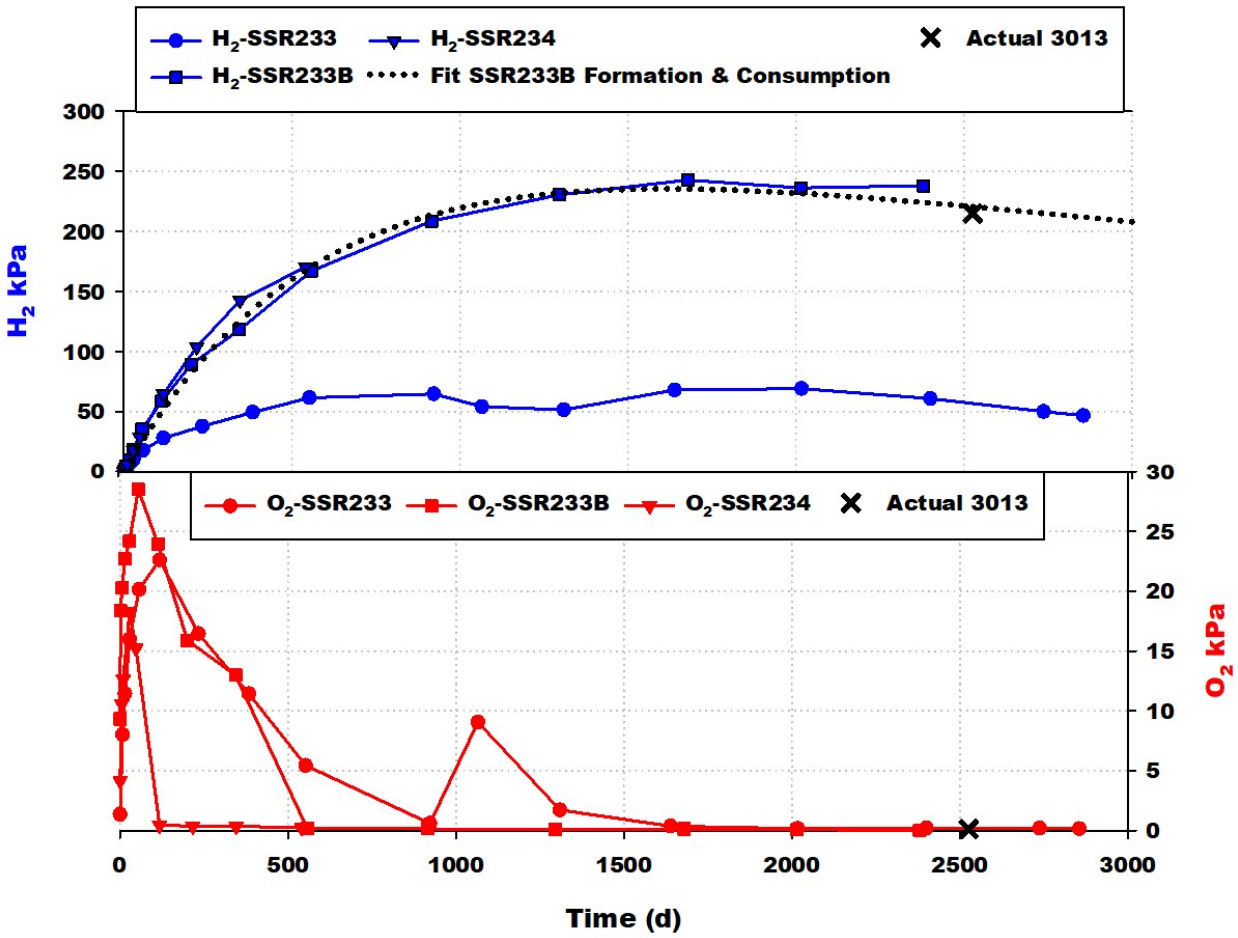

Figure 23. Partial pressures of hydrogen and oxygen as a function of time in three SSRs loaded with H003328 material.

3.5 Consumption of Water and RH Behavior

The hydrogen gas generation in both high-purity oxides and salt-bearing material is dependent upon the amount of water available for radiolysis. The available water for radiolysis in both cases follows the RH. In the case of high-purity oxides, the RH is related to the monolayer coverage of physisorbed water. Water that is converted to a chemisorbed form such as a hydroxyl does not contribute to the RH. Hydroxyls are not thought to participate in radiolysis. In the case of salts, the RH increases as the salt picks up waters of hydration when exposed to moisture and then jumps up as the salt deliquesces. With

continued exposure after deliquescence, the RH increases as the salt concentration of the resulting liquid decreases. After packaging, radiolysis destroys water, but the loss of water as measured by the RH is much larger than the radiolysis of water to form hydrogen.

The RH in containers with high-purity oxides decreases uniformly. The rate of consumption increases with the specific power and decreases with higher amounts of initial water content as shown in Figure 24 and Figure 25. The RH trends to zero at long times in both large- and small-scale experiments. The rapid initial decrease in RH is not due to radiolysis. A relatively rapid conversion of physisorbed water to chemisorbed water occurs initially until one monolayer of chemisorbed water is formed. The rate of decline generally decreases with water loss and is split between radiolysis and further formation of chemisorbed water.

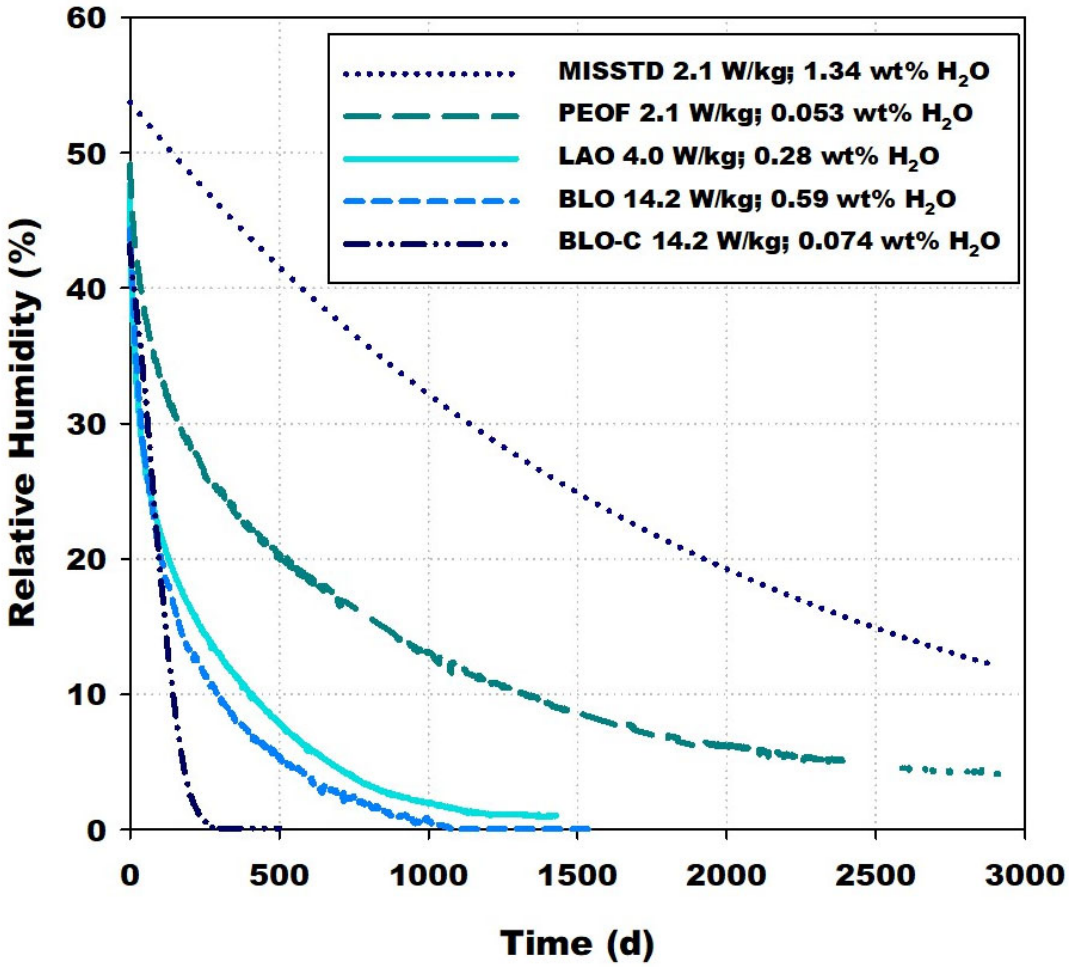

Figure 24. The RH behavior for high-purity oxides exposed to 55% RH and loaded in SSRs.

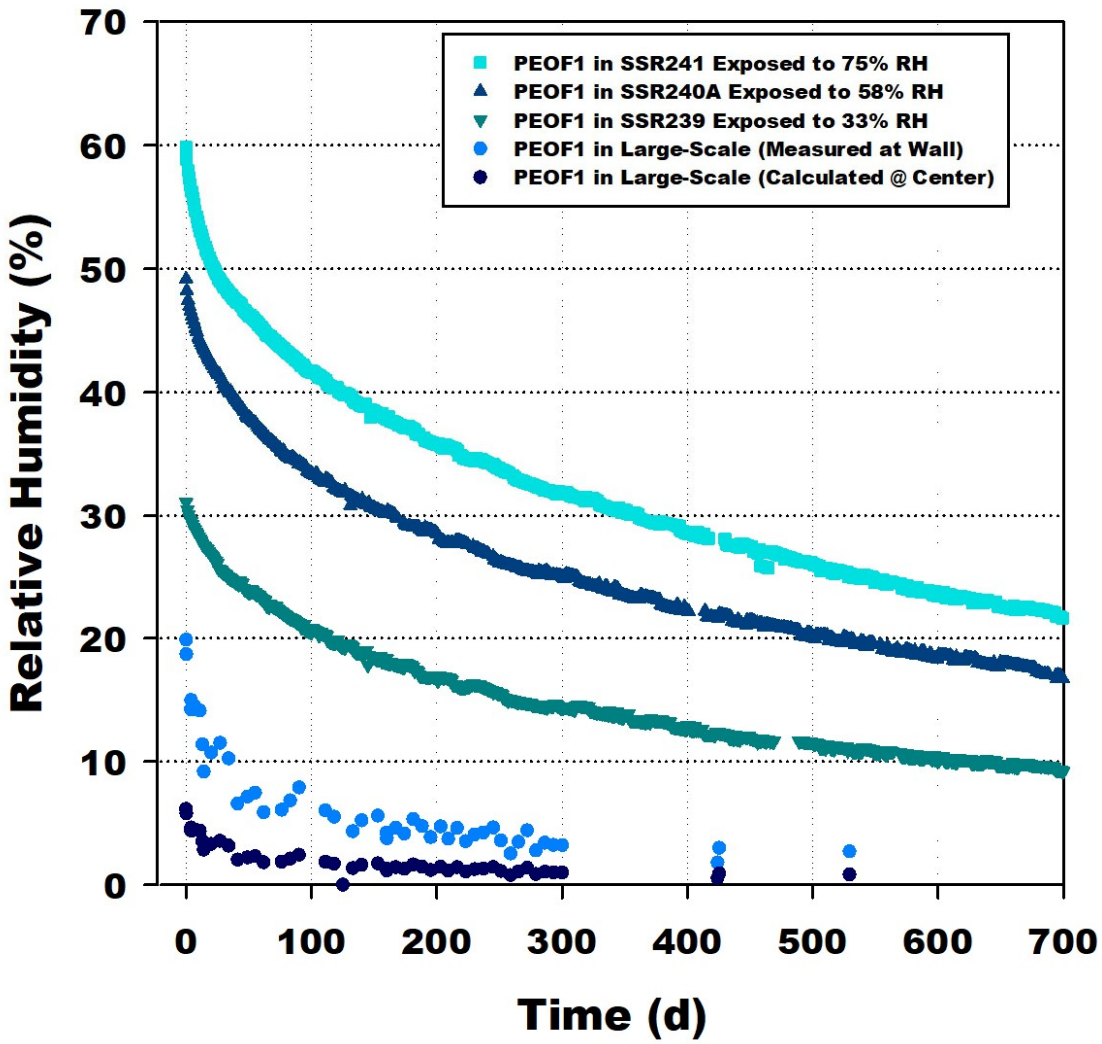

Figure 25. The RH behavior for high-purity oxide material PEOF1 exposed to various RH and loaded in SSRs and a large-scale container.

In the case of salts, a different picture emerges. An initial rapid decline in RH is common in both cases, but after that decline the salt RH tends to stabilize for long periods of time (Figure 26). When there is sufficient water to form deliquescent liquids, the RH is pinned at the deliquescent RH until the water is consumed, which can take years as shown by Figure 27 and Figure 28. Consumption of water appears to be mainly by radiolysis to form hydrogen and HCl.

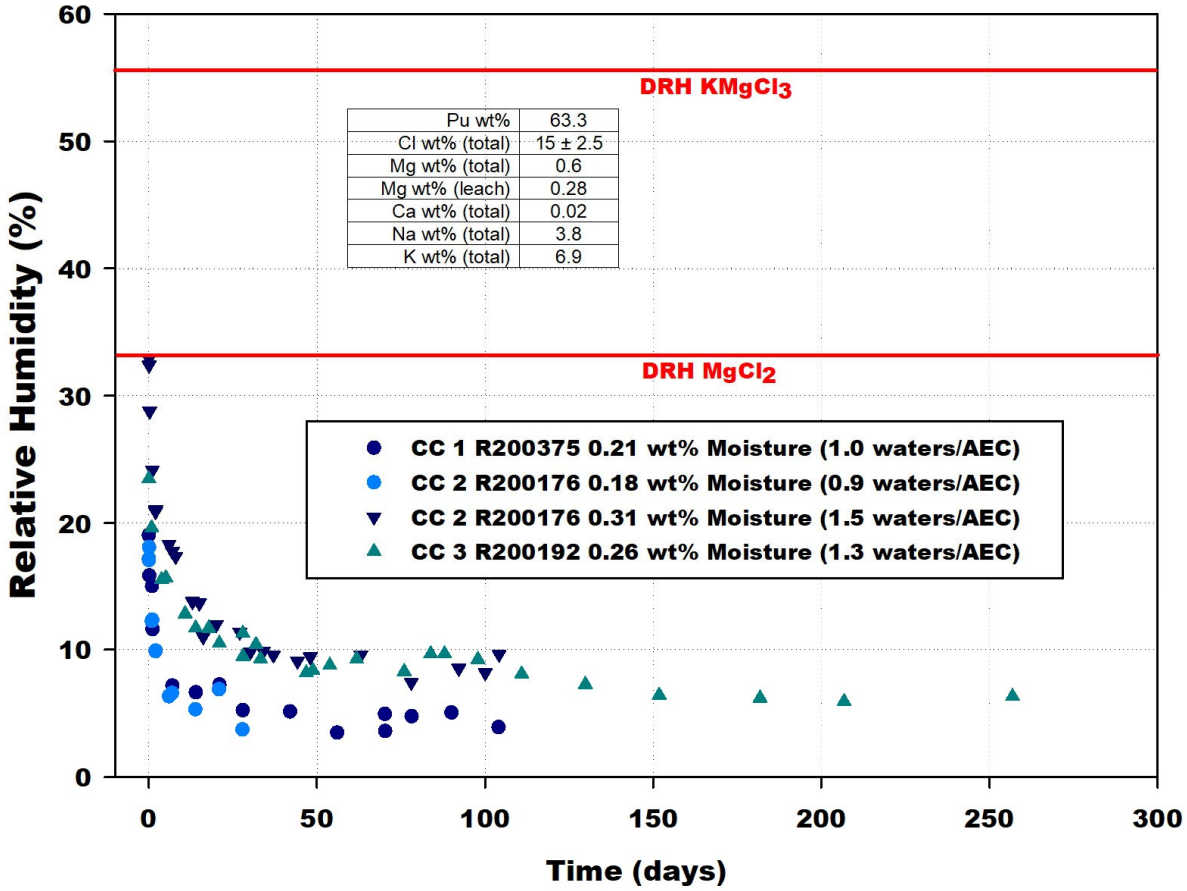

Figure 26. The RH behavior for multiple large-scale loadings of the Masterblend, a chloride salt-bearing impure oxide material, with different water loadings. After an initial rapid decrease, the RH stabilizes as it is controlled by hydrated alkaline earth chlorides present in the material matrix.

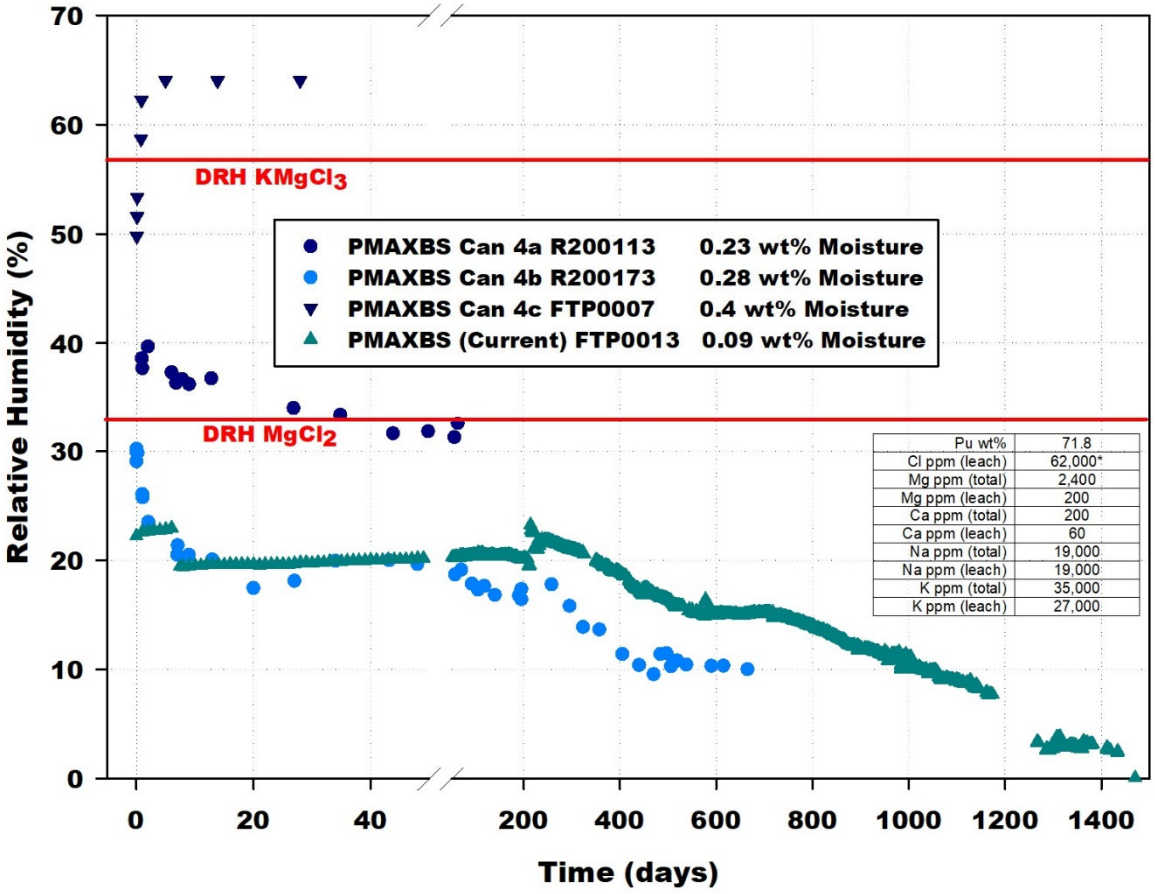

Figure 27. The RH behavior for multiple loadings of the PMAXBS, a chloride salt-bearing impure oxide material. After an initial rapid decrease, the RH at the sensor is pinned at specific RH due to hydrated or deliquesced salts in the material matrix. As the water is consumed by radiolysis, the RH drops or is pinned at a lower value for the next lower hydrate.

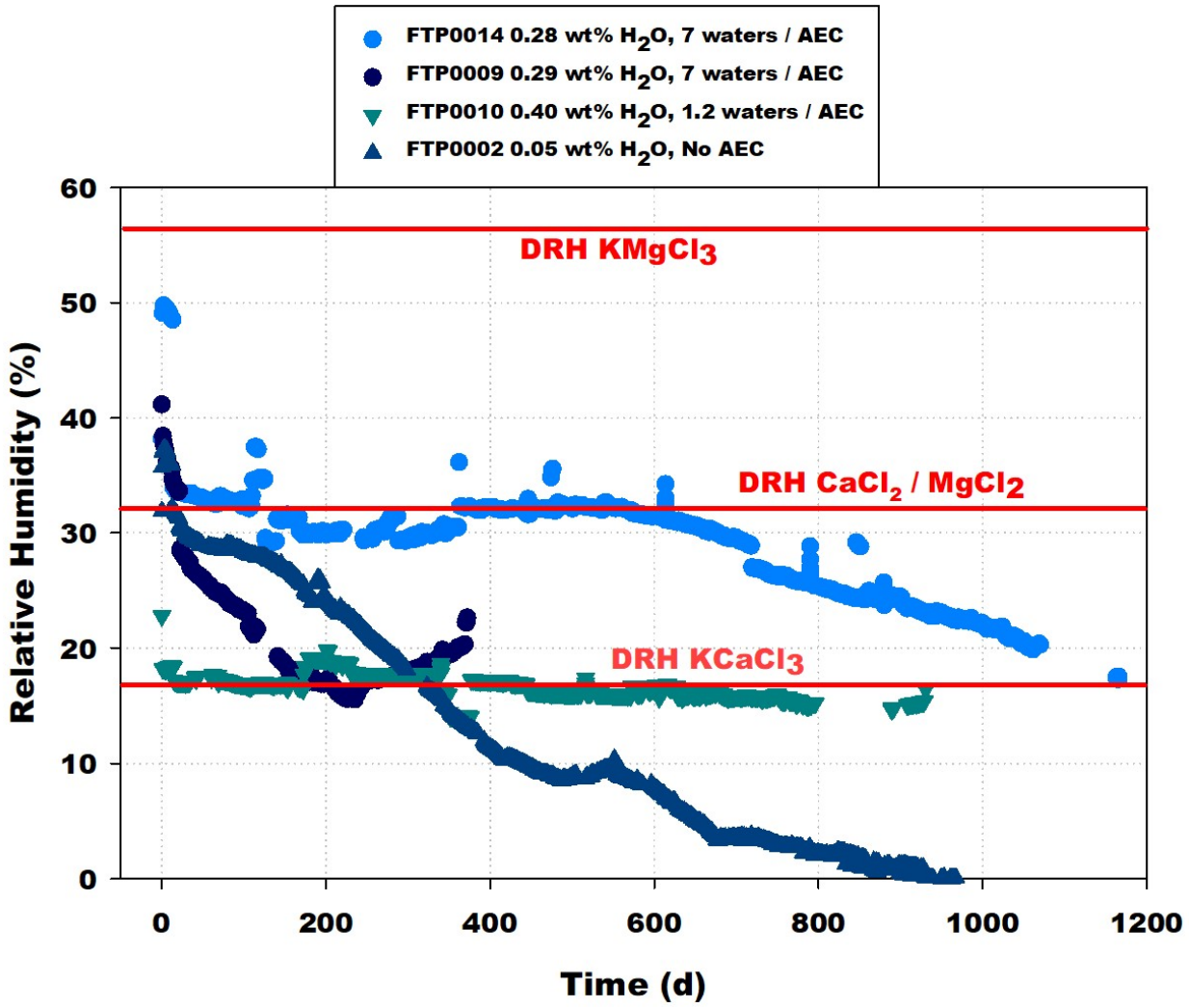

Figure 28. RH in the Large-Scale Corrosion Series II containers including Low Ca (FTP0014), Low Mg (FTP0009), High Ca (FTP0010), and the base material (FTP0002). After an initial rapid decrease, the RH at the sensor is pinned at specific RH due to hydrated or deliquesced alkaline earth chloride (AEC) salts in the material matrix. As the water is consumed by radiolysis, the RH drops or is pinned at a lower value for the next lower hydrate.

4 Conclusions

Shelf-life surveillance experiments have been conducted on a variety of high-purity and impure plutonium oxide materials. MIS represented materials were tested at the 3013 Standard bounding limit of 0.5 wt.% moisture achieved by vapor adsorption. The observed gas generation behavior is described by models that include both the formation and consumption of hydrogen and result in much lower pressures than those that would be expected from the complete radiolysis of water without the consumption of hydrogen. High-purity oxides generate hydrogen that is later consumed to an equilibrium pressure or to zero. The data suggest that material stabilized and immediately packaged would favor complete consumption as the adsorbed water is eventually consumed. The possibility exists for flammable mixtures of hydrogen and oxygen to form in packages with high specific power materials with moisture levels approaching the limit for the 3013 Standard. Some high-purity mixed Pu-U oxides exhibited higher rates of moisture adsorption than high-purity Pu oxides, which can be explained by the formation of hydrated UO_3; however, the gas generation behavior of high purity mixed Pu-U oxides is similar to and bounded by the behavior of high-purity Pu oxides.

Moisture adsorption on salt-bearing impure Pu oxides forms hydrated salt compounds. The hydration can occur rapidly and can result in the formation of liquid phases in the material. The gas generation behavior of the hydrated salt-bearing impure Pu oxides is also described by models that include the formation and consumption of hydrogen but results in higher hydrogen partial pressures than those observed in containers with high purity Pu and Pu-U mixed oxides. The hydrogen partial pressures in salt-bearing impure Pu oxides can remain near the maximum pressure for many years. The possibility for generating flammable mixtures of hydrogen and oxygen exists for impure oxide materials with alkaline earth chloride salts having between two and seven waters of hydration and a total moisture content above 0.3 wt.%. However, the data for the consumption of oxygen in the shelf-life experiments provides sufficient evidence that any flammable mixtures that may have formed in actual 3013 containers are no longer present.

Consumption of water measured through RH occurs in all materials as hydrogen is formed. The consumption occurs the fastest in high-purity oxides, particularly those materials with higher specific power. The RH inside containers with salt-bearing impure oxides may be pinned at specific RH for long periods of time, is controlled by hydrated salt compounds, and could support corrosion. However, the RH eventually decreases with time as the water is consumed to form hydrogen.

Experiments performed with the same materials in both large-and small-scale experiments produce similar results for the generation of headspace gases and the consumption of water. The higher pressures obtained with the small-scale experiments with representative materials show that the results of those experiments bound the storage population of 3013 containers. Scaling corrections may be performed on data collected from MIS represented materials loaded in small-scale experiments at the bounding moisture, and the results from the SSR experiments can be used to predict the behavior of hydrogen gas generation in 3013 containers if the free-gas volume and amount of water is known.

5 References

(1) U. S. Department of Energy. *Stabilization, Packaging, and Storage of Plutonium-Bearing Materials*; DOE-STD-3013-94; Washingon, D.C., 1994.

(2) U. S. Department of Energy. *Criteria for Preparing and Packaging Plutonium Metals and Oxides for Long-Term Storage*; DOE-STD-3013-96; Washingon, D.C., 1996.

(3) U. S. Department of Energy. *Stabilization, Packaging, and Storage of Plutonium-Bearing Materials*; DOE-STD-3013-2000; Washingon, D.C., 2000.

(4) Bailey, G.; Bluhm, E.; Lyman, J.; Mason, R.; Paffett, M.; Polansky, G.; Roberson, G. D.; Sherman, M.; Veirs, K.; Worl, L. *Gas Generation from Actinide Oxide Materials*; LA-13781-MS; Los Alamos National Laboratory, Los Alamos, NM, 2000.

(5) Worl, L.; Berg, J.; Bielenberg, P. A.; Carrillo, A.; Martinez, M.; Montoya, A.; Veirs, D.; Puglisi, C. V.; Rademacher, D.; Schwartz, D.; et al. *Shelf Life Surveillance for PuO2 Bearing Materials FY04 Second Quarterly Report*; LA-UR-04-4228; Los Alamos National Laboratory, Los Alamos, NM, 2004.

(6) Berg, J.; English, D.; Harradine, D.; Hill, D.; McFarlan, J.; Padilla, D.; Prenger, C.; McInroy, R.; Morris, J.; Veirs, D.; et al. *MIS Small and Large Scale Sample Surveillance 2002 Year End Status Report*; LA-UR-02-7356; Los Alamos National Laboratory, Los Alamos, NM, 2002.

(7) Narlesky, J.; Berg, J.; Duque, J. G.; Harradine, D.; Hill, D.; Kaczar, G.; Lillard, R. S.; Lopez, A.; Martinez, M.; Peppers, L.; et al. *Surveillance and Monitoring Program Full-Scale Experiments to Evaluate the Potential for Corrosion in 3013 Containers*; LA-UR-17-30653; Los Alamos National Laboratory, Los Alamos, NM, 2017.

(8) Bielenberg, P. A.; Prenger, F. C.; Veirs, D. K.; Jones, G. F. Effects of pressure on thermal transport in plutonium oxide powder. *International Journal of Heat and Mass Transfer* **2006**, *49*, 3229-3239.

(9) Erickson, R. M. *Representation of Items Packaged to DOE-STD-3013-2000*; LA-14016-MS; Los Alamos National Laboratory, Los Alamos, NM, 2003.

(10) Duffey, J. M.; Veirs, D. K.; Berg, J. M.; Livingston, R. R. Pressure Development in Sealed Containers with Plutonium-bearing Materials. *Journal of Nuclear Material Management* **2010**, *37* (3), 32-42.

(11) Veirs, D. K.; Stroud, M. A.; Martinez, M. A.; Carrillo, A.; Berg, J. M.; Narlesky, J. E.; Simms, L.; Worl, L. A. *MIS High-Purity Plutonium Oxide Oxalate Precipitation/Calcination Product PBO-47-09-012-023: Final Report*; Los Alamos National Laboratory, 2019. http://permalink.lanl.gov/object/view?what=info:lanl-repo/lareport/LA-UR-19-31446.

(12) Veirs, D. K.; Stroud, M. A.; Berg, J. M.; Narlesky, J. E.; Worl, L. A.; Martinex, M. A.; Carillo, A. *MIS High-Purity Plutonium Oxide Hydride Product 5501579 (SSR124): Final Report*; Los Alamos National Laboratory, 2018. http://permalink.lanl.gov/object/view?what=info:lanl-repo/lareport/LA-UR-18-20970.

(13) Narlesky, J. E.; Veirs, D. K.; Berg, J. M.; Carrillo, A.; Martinez, M.; Worl, L. A. *MIS Shelf-Life Final Report for Plutonium-Uranium Oxide Item 669194 (SSR126) from Rocky Flats Special Assembly Operations*; Los Alamos National Laboratory, 2023. http://permalink.lanl.gov/object/view?what=info:lanl-repo/lareport/LA-UR-22-30655.

References

(14) Narlesky, J. E.; Veirs, D. K.; Berg, J. M.; Carrillo, A.; Martinez, M.; Worl, L. A. *MIS Shelf-Life Final Report for Plutonium-Uranium Oxide Item PSU-84-06-05 (SSR133) from Hanford Polycube Oxidation*; Los Alamos National Laboratory, 2022. http://permalink.lanl.gov/object/view?what=info:lanl-repo/lareport/LA-UR-22-30458.

(15) Veirs, D. K.; Stroud, M. A.; Martinez, M.; Carrillo, A.; Berg, J. M.; Narlesky, J. E.; Worl, L. A. *MIS High-Purity Plutonium/Uranium Oxide Hydride Product 5501407 (SSR129): Final Report*; Los Alamos National Laboratory, 2019. http://permalink.lanl.gov/object/view?what=info:lanl-repo/lareport/LA-UR-19-20826.

(16) Veirs, D. K.; Stroud, M. A.; Martinez, M.; Carrillo, A.; Berg, J. M.; Narlesky, J. E.; Worl, L. A. *MIS High-Purity Uranium/Plutonium Oxide Metal Oxidation Product SCP711-56 (SSR135): Final Report*; Los Alamos National Laboratory, 2019. http://permalink.lanl.gov/object/view?what=info:lanl-repo/lareport/LA-UR-19-20356.

(17) Narlesky, J. E.; Veirs, D. K.; Berg, J. M.; Carrillo, A.; Martinez, M. A.; Worl, L. A. *MIS Shelf-Life Final Report for Plutonium Oxide Item CAN92 (SSR147) from Rocky Flats Analytical Laboratory Operations*; Los Alamos National Laboratory, 2022. http://permalink.lanl.gov/object/view?what=info:lanl-repo/lareport/LA-UR-22-29337.

(18) Narlesky, J. E.; Veirs, D. K.; Berg, J. M.; Carrillo, A.; Martinez, M.; Stroud, M. A.; Worl, L. A. *MIS Shelf-Life Final Report for SSR154: High-Purity Plutonium Oxide Item ARF-102-85-114-1*; Los Alamos National Laboratory, 2022. http://permalink.lanl.gov/object/view?what=info:lanl-repo/lareport/LA-UR-22-30236.

(19) Veirs, D.; Kruk, I.; Narlesky, J.; Martinez, M.; Carrillo, A.; Berg, J.; Worl, L. *MIS Plutonium Oxide with Low Fluoride from Peroxide Precipitation/Calcination Product 07161856 (SSR122): Final Report*; LA-UR-21-30452; Los Alamos National Laboratory, Los Alamos, NM, 2021.

(20) Veirs, D.; Stroud, M. A.; Berg, J.; Narlesky, J.; Worl, L.; martinez, M. A.; Carrillo, A. *MIS High-Purity Plutonium Oxide Metal Oxidation Product TS707001 (SSR123): Final Report*; LA-UR-17-27172; Los Alamos National Laboratory, Los Alamos, NM, 2017.

(21) Veirs, D. K.; Stroud, M. A.; Martinez, M.; Carrillo, A.; Berg, J. M.; Narlesky, J. E.; Worl, L. A. *MIS High-Purity Plutonium Oxide Metal Oxidation Product BLO-39-11-14-004 (SSR132 and 132A): Final Report*; Los Alamos National Laboratory, 2018. http://permalink.lanl.gov/object/view?what=info:lanl-repo/lareport/LA-UR-18-26650.

(22) Stroud, M. A.; Veirs, D. K.; Narlesky, J. E.; Berg, J. M.; Romero, E. L.; Rios, D.; Wilson, K. V., Jr.; Worl, L. A. *Investigating the Dependence of Hydrogen and Oxygen Generation from High-Purity Plutonium Oxides in Sealed Containers*; Los Alamos National Laboratory, 2019. http://permalink.lanl.gov/object/view?what=info:lanl-repo/lareport/LA-UR-19-27487.

(23) Veirs, D. K.; Berg, J. M.; Hill, D. D.; Harradine, D. M.; Narlesky, J. E.; Romero, E. L.; Trujillo, L.; Wilson, K. V. *Water radiolysis on plutonium dioxide: Initial results identifying a threshold relative humidity for oxygen gas generation*; LA-UR-12-26423; Los Alamos National Laboratory, Los Alamos, NM, 2012.

(24) Veirs, D.; Kruk, I.; Narlesky, J.; Martinez, M. A.; Carrillo, A.; Berg, J.; Worl, L. *MIS Plutonium oxide with chloride salts from pyrochemical processes product 520610020 (SSR139); Final Report*; LA-UR-20-29362; Los Alamos National Laboratory, Los Alamos, NM, 2020.

(25) Veirs, D. K.; Kruk, I. I.; Narlesky, J. E.; Martinez, M. A.; Carrillo, A.; Berg, J. M.; Worl, L. A. *MIS plutonium oxide with chloride salts content from pyrochemical processes product 520610020 (SSR139); Final Report*; Los Alamos National Laboratory, 2020. http://permalink.lanl.gov/object/view?what=info:lanl-repo/lareport/LA-UR-20-29362.

References

(26) Narlesky, J. E.; Stroud, M. A.; Smith, P. H.; Wayne, D. M.; Mason, R. E.; Worl, L. A. *Characterization of Representative Materials in Support of Safe, Long Term Storage of Surplus Plutonium in DOE-STD-3013 Containers*; LA-UR-12-23790; Los Alamos National Laboratory, Los Alamos, NM, 2012.

(27) Narlesky, J.; Veirs, D.; Stroud, M. A.; Berg, J.; Kulis, J.; Romero, E. L.; Rios, D.; Wilson, K. V.; Worl, L. Investigating the Dependence of Hydrogen Generation from High-Purity Plutonium Oxides on Radiolysis. In *Plutonium Futures–The Science 2018*, San Diego, CA, 2018; 2018.

(28) Veirs, D.; Stroud, M. A.; Narlesky, J.; Berg, J.; Romero, E. L.; Rios, D.; Wilson, K. V.; Worl, L. Investigating the Dependence of Hydrogen and Oxygen Generation from High-Purity Plutonium Oxides in Sealed Containers. In 19th International Symposium on the Packaging and Transportation of Radioactive Materials,, New Orleans, LA; 2019.

(29) Veirs, D. K.; Berg, J. M.; Crowder, M. L. *The effect of plutonium dioxide water surface coverage on the generation of hydrogen and oxygen*; LA-UR-12-22377; Los Alamos National Laboratory, Los Alamos, NM, 2012.

(30) Veirs, D.; Berg, J.; Stroud, M. A. *Obtaining G-values and Rate Constants from MIS Data*; LA-UR-17-23787; Los Alamos National Laboratory, Los Alamos, NM, 2017.

(31) Thein, S. M.; Bereolos, P. J. *Thermal Stabilization of $^{233}UO_2$, $^{233}UO_3$, and $^{233}U_3O_8$*; ORNL/TM-2000/82; Oak Ridge National Laboratory, Oak Ridge, TN, 2000.

(32) Tamasi, A. L.; Boland, K. S.; Czerwinski, K.; Ellis, J. K.; Kozimar, S. A.; Martin, R. L.; Pugmire, A., L.; Reilly, D.; Scott, B. L.; Sutton, A. D.; et al. Oxidation and Hydration of U_3O_8 Materials Following Controlled Exposure to Temperature and Humidity. *Anal. Chem.* **2015**, *87*, 4210-4217.

(33) Harrington, C. D.; Ruehle, A. *Uranium Production Technology*; D. Van Nostrand Company, Inc., 1959.

(34) Berg, J. M.; Garcia, E.; Long, G.; Martinez, M. A.; Narlesky, J. E.; Veirs, D. K.; Williams, C.; Worl, L. A. *The effect of moisture content on oxygen generation for 011589A substitute materials*; LA-UR-08-2546; Los Alamos National Laboratory, Los Alamos, NM, 2008.

(35) Duque, J. G.; Stroud, M. A.; Narlesky, J. E.; Rios, D.; Kelly, E. J.; Joyce, S. A.; Berg, J. M.; Veirs, D. K.; Worl, L. A. *Microscopic Characterization of Corrosion of Teardrop Specimens Exposed to Plutonium-Bearing Materials with Calcium Chloride Impurities*; Los Alamos National Laboratory, 2019. http://permalink.lanl.gov/object/view?what=info:lanl-repo/lareport/LA-UR-19-28748.

(36) Rios, D.; Gaunt, A.; Narlesky, J.; Berg, J.; Veirs, D.; Worl, L. *Capture, Identification and Quantification of the Elusive Chlorine-Containing Gases Emitted from Hydrated PuO2/Salt Mixtures*; LA-UR-17-27871; Los Alamos National Laboratory, Los Alamos, NM, 2017.

(37) Rios, D.; Gaunt, A.; Narlesky, J.; Berg, J.; Veirs, D.; Worl, L. *Lack of Corrosion and Chlorine-Containing Gas Generation from Once Corrosive Hanford High Moisture Material*; LA-UR-20-25325; Los Alamos National Laboratory, Los Alamos, NM, 2020.

(38) Venetz, T. J.; McClard, J. W.; Berg, J. M.; Narlesky, J. E.; Veirs, D. K. *Evaluation of Hanford Item Potentially Packaged in Excess of DOE-STD-3013 limit for Moisture*; HNF-EDC-08-39285; Hanford, Richland, WA, 2008.

(39) Veirs, D.; Kelly, E.; Berg, J.; Nguyen, B.; McClard, C.; Hensel, S.; Duffey, J. M.; Scogin, J. H. *Gas Composition Observed by Destructive Examination of 3013 Containers*; Los Alamos National Laboratory, Los Alamos, NM, 2023.

References

(40) Veirs, D. K.; Berg, J. M.; Stroud, M. A. *Obtaining G-values and rate constants from MIS data*; LA-UR-17-23787; Los Alamos National Laboratory, Los Alamos, NM, 2017.

6 Acknowledgments

Funding for this work was provided to the MIS Program by the Assistant Manager for Nuclear Materials Stabilization, Savannah River Operations Office, Department of Energy's Office of Environmental Management. This report summarizes many years of work by many individuals. We are especially grateful to the PF-4 technicians who keep these experiments running for years: Max Martinez, Alex Carillo, Leonardo Trujillo, Kennard Wilson, Justin Watson, and Mike Poole.

Appendix A: Experimental Details for Large-Scale Shelf-Life Studies

The large-scale shelf-life studies were conducted inside modified British Nuclear Fuel, Limited (BNFL) 3013 inner containers. The design of the large-scale container system has been described previously. [6] The container body was manufactured by Westinghouse Engineered Products Division (EPD), which also produced the Hanford inner 3013 containers. The containers are constructed from 316L stainless steel and have an internal volume of nominally 2.3 liters. Up to 5,000 g of oxide material may be loaded into the containers, but administrative requirements limit the amount of Pu to 4,400 g per container. The large-scale modified 3013 container assembly consists of container body, container lid, and rupture disk (burst disk). These components are shown in Figure 29. The large-scale container uses a modified lid that includes a fitting that attaches to a gas manifold used to perform gas sampling for gas chromatography (GC). The center of the lid has a threaded hole where the burst disk is installed. A gas tungsten arc weld (GTAW) is used to attach the container lid to the body prior to loading material. The container body has feedthroughs for thermocouples and various electrical components such as relative humidity (RH) sensors installed within the container. The container body in some designs also includes a Raman spectroscopy chamber for *in situ* gas sampling.

Twelve large-scale surveillance containers were loaded for gas generation and corrosion studies using test materials with added moisture. The materials were calcined to the desired temperature prior to loading. A moisture measurement was performed to determine the initial moisture (by LOH-200 °C or by TGA-MS). The desired moisture content was achieved by flowing humidified gas through the container loaded with the test material or by exposing the test material to a humid atmosphere inside the static enclosure surrounding a balance prior to loading. The total adsorbed moisture was determined by adding the initial moisture on the material to the moisture adsorbed by the material during humidification.

Moisture addition by humidified gas flow was performed in the following way [5]. The test material was loaded into the container by pouring through the burst disk hole, and the burst disk was installed to seal the hole. The caps were removed from the gas manifold on the lid and from the port for the Raman spectroscopy chamber, and the container attached to the helium gas supply at the Raman spectroscopy chamber port. The container was placed on a balance to measure the weight gain with time, and water was added by flowing a humidified stream of helium through the container from the bottom to the top. The humid gas flow was stopped when the desired (or maximum) weight gain was achieved. The container was disconnected from the gas manifold, and all ports on the container were then sealed closed.

Moisture addition by vapor adsorption using the humidified balance enclosure was performed in the following way[7]. The test materials were poured into a stainless steel Vollrath pan (20.75 x 12.75 in), and the pan with the test material was placed on the balance inside the enclosure. A saturated solution was placed in a shallow dish inside of the enclosure (see Figure 30). A Vaisala HMT333 series humidity and temperature sensor and transmitter was installed in the port on top of the enclosure to measure RH and temperature. Thermocouples were placed at various locations inside the enclosure, such as inside the material and under the metal pan. Temperature, RH, and the mass of the material were recorded continuously during exposure. The enclosure was opened when the total adsorbed moisture reached the desired (or maximum) weight gain. The test material was immediately placed in the instrumented 3013 inner container by pouring the material through the threaded hole in the lid. The burst disk was installed and sealed to the container lid, and all ports on the container were sealed closed.

Appendix A: Experimental Details for Large-Scale Shelf-Life Studies

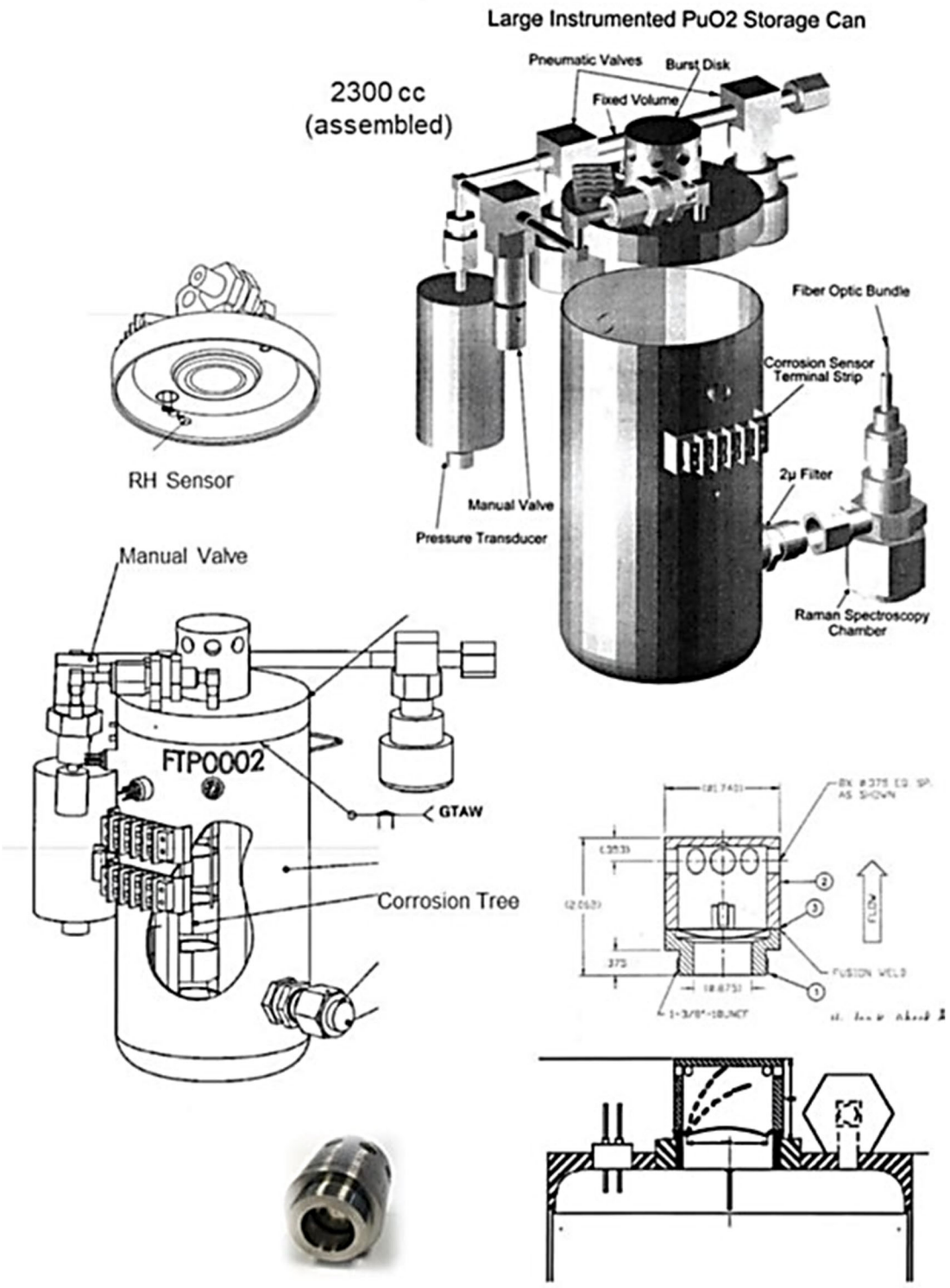

Figure 29. The 2.3 liter large-scale surveillance container with external components and burst disk. The container body and lid are constructed from 316L stainless steel. The assembled container is approximately 9 inches tall and 4 inches in diameter.

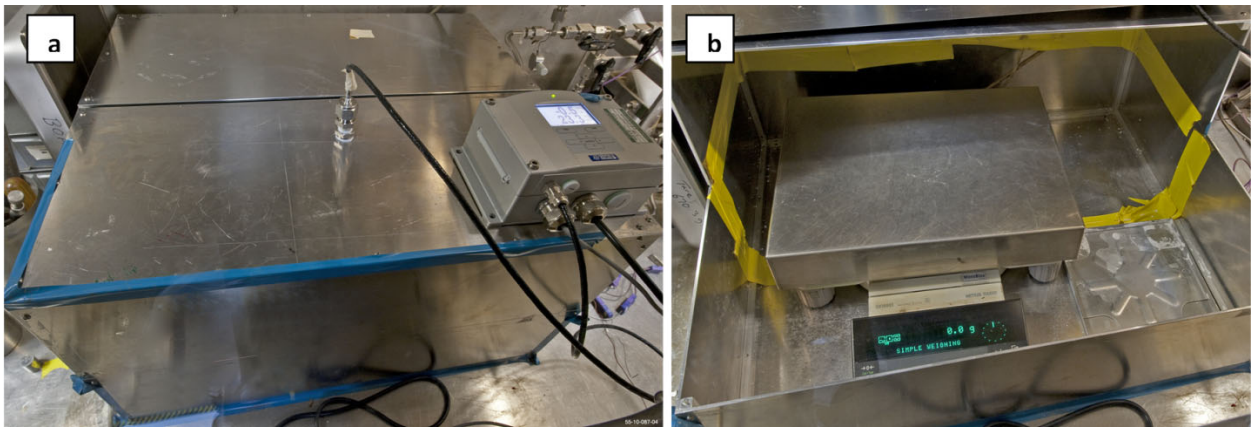

Figure 30. Humidified balance enclosure used to expose test materials to a high RH environment for moisture addition by vapor adsorption. (a) Outside of enclosure with lid closed. (b) Inside of enclosure with lid removed.

The containers were installed on the large-scale array by connecting the container to the gas manifold and connecting the instrumentation. The container pressure, water vapor pressure and the temperature at various locations in the container were monitored throughout the experiment. The gas composition inside the containers was determined by gas chromatography and/or Raman spectroscopy at scheduled intervals. A complete list of the large-scale experiments is given in Table 4.

Appendix A: Experimental Details for Large-Scale Shelf-Life Studies

Table 4. Large-scale container experiments conducted at LANL. Containers indicated as “reload” were removed from the array, opened, and had additional moisture added.

ID	Material	Description	Pu	H_2O	Hydration Method	Report Reference
			(wt. %)	(wt. %)		LA-UR-
R200145	PEOF1	Oxalate Precipitation Product (LANL)	87.5	0.03	Humidified Gas Flow	04-4228
R200113	PMAXBS	Oxide from Pyrochemical Processes (LANL)	71.8	0.19	Humidified Gas Flow	04-4228
R200113 reload	PMAXBS	Oxide from Pyrochemical Processes (LANL)	71.8	0.23	Humidified Gas Flow	17-30653
R200173	PMAXBS	Oxide from Pyrochemical Processes (LANL)	71.8	0.23	Humidified Gas Flow	17-30653
FTP0007	PMAXBS	Oxide from Pyrochemical Processes (LANL)	71.8	0.40	Exposure to liquid water (water dish placed inside loaded container)	17-30653
FTP0013	PMAXBS	Oxide from Pyrochemical Processes (LANL)	71.8	0.09	Humidified Balance	17-30653
R200375	MASTERBLEND	LS Corrosion Series I (2006)	63.3	0.21	Humidified Gas Flow	
R200176	MASTERBLEND	LS Corrosion Series I (2006)	63.3	0.18	Humidified Gas Flow	
R200176 reload	MASTERBLEND	LS Corrosion Series I (2006)	63.3	0.31	Humidified Gas Flow	
R200192	MASTERBLEND	LS Corrosion Series I (2006)	63.3	0.26	Humidified Gas Flow	
FTP0002	MOD. MASTERBLEND II	LS Corrosion Series II (2009) Base Material (no AEC added)	75.8	0.05	Humidified Balance	17-30653
FTP0014	Low Ca MOD. MASTERBLEND II	LS Corrosion Series II (2009) Base Material (0.34 wt.% $KCaCl_3$ added)	75.5	0.28	Humidified Balance	17-30653
FTP0009	Low Mg MOD. MASTERBLEND II	LS Corrosion Series II (2009) Base Material (0.34 wt.% $KCaCl_3$ added)	75.5	0.29	Humidified Balance	17-30653
FTP0010	High Ca MOD. MASTERBLEND II	LS Corrosion Series II (2009) Base Material (3.4 wt.% $KCaCl_3$ added)	72.4	0.40	Humidified Balance	17-30653
FTP0003	High Mg MOD. MASTERBLEND II	LS Corrosion Series II (2009) Base Material (3.4 wt.% $KCaCl_3$ added)	72.4	0.56	Humidified Balance	17-30653
FTP0011	LAO	Peroxide Precipitation Product (LANL)	87.8	0.32	Humidified Balance	
FTP0011 reload	LAO	Peroxide Precipitation Product (LANL)	87.8	0.58	Addition of liquid water to material	

Appendix B: Experimental Details for Small-Scale Shelf-Life Studies

The small-scale shelf-life studies were conducted with small-scale reactors (SSRs). The design of the SSR system has been described previously.[6] The container's nominally 5 cm^3 internal volume is scaled to ~1/500th of the inner 3013 storage container. The container is approximately 2.5 inches tall and 0.5 inches in diameter. The material of construction of the SSR is 304L stainless steel. The SSR consists of a container body welded into a Conflat flange and a lid consisting of a Conflat flange with tubing attachments for connections to a pressure transducer and a gas manifold. A 304L stainless steel inner bucket is used to hold the material and is inserted into the container body during the loading activities. The inner bucket allows the fine plutonium oxide powder to be handled with minimal or no spillage. A low-internal-volume pressure transducer and associated low-volume tubing is attached to the lid. The gas sampling volume located between the two sampling valves is 0.05 cm^3 (~1 % of the SSR volume) and allows gas composition to be determined with minimal effect on the internal gas pressure.

Small-scale reactors have interchangeable parts with varying volumes. The eight different types of SSRs are listed in Table 5 along with the interchangeable components and total internal volume.[40] The type H SSR shown in Figure 31 was the original design and included the standard lid, 2 ¾ in (Tall) Conflat bottom, and an Ashcroft K1 pressure transducer (100 psi range). The Ashcroft K1 transducers are not absolute and require a correction to the data. Therefore, the Omega PX429, which are absolute pressure transducers were later identified as a replacement.

A modified version of the lid that includes a RH sensor was later developed. The spacing required to accommodate the RH sensor increased the volume of the SSR, so the 2 in (Short) Conflat bottom was developed to maintain a more consistent volume in the experiments. However, it was found that the RH sensor protruded down into the inner bucket and often did not allow for loading the 10 g of material required for the experiments. Therefore, the type C SSR shown in Figure 32 was used for experiments requiring RH measurements.

Table 5. SSR Designs and Internal Volumes.

Container Type	Lid Design	Bottom Type	Pressure Transducer	SSR Internal Volume (mL)
A	RH	Short	Omega PX429	5.232
B	Standard	Short	Omega PX429	4.520
C	RH	Tall	Omega PX429	6.145
D	Standard	Tall	Omega PX429	5.433
E	RH	Short	Ashcroft K1	5.125
F	Standard	Short	Ashcroft K1	4.413
G	RH	Tall	Ashcroft K1	6.038
H	Standard	Tall	Ashcroft K1	5.326

Appendix B: Experimental Details for Small-Scale Shelf-Life Studies

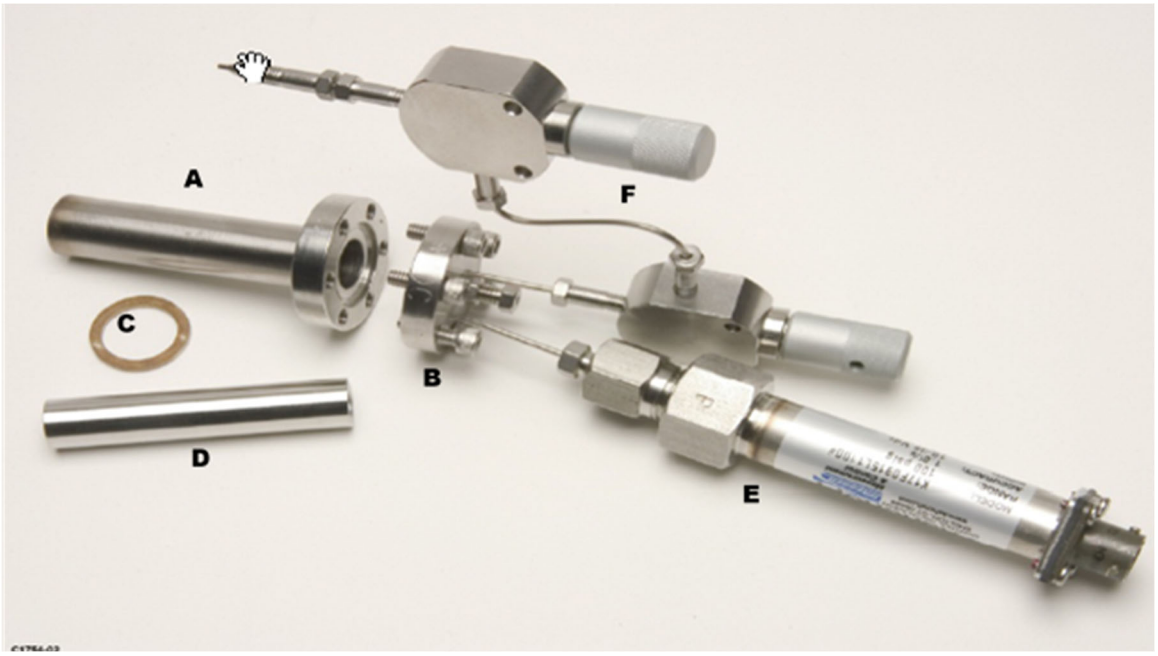

Figure 31. Disassembled example of a Type H SSR: Conflat container body (A) with Conflat flange lid (B), copper gasket (C), inner bucket (D), pressure transdducer (E), and a sampling volume between two sampling valves with connection to the gas manifold (F).

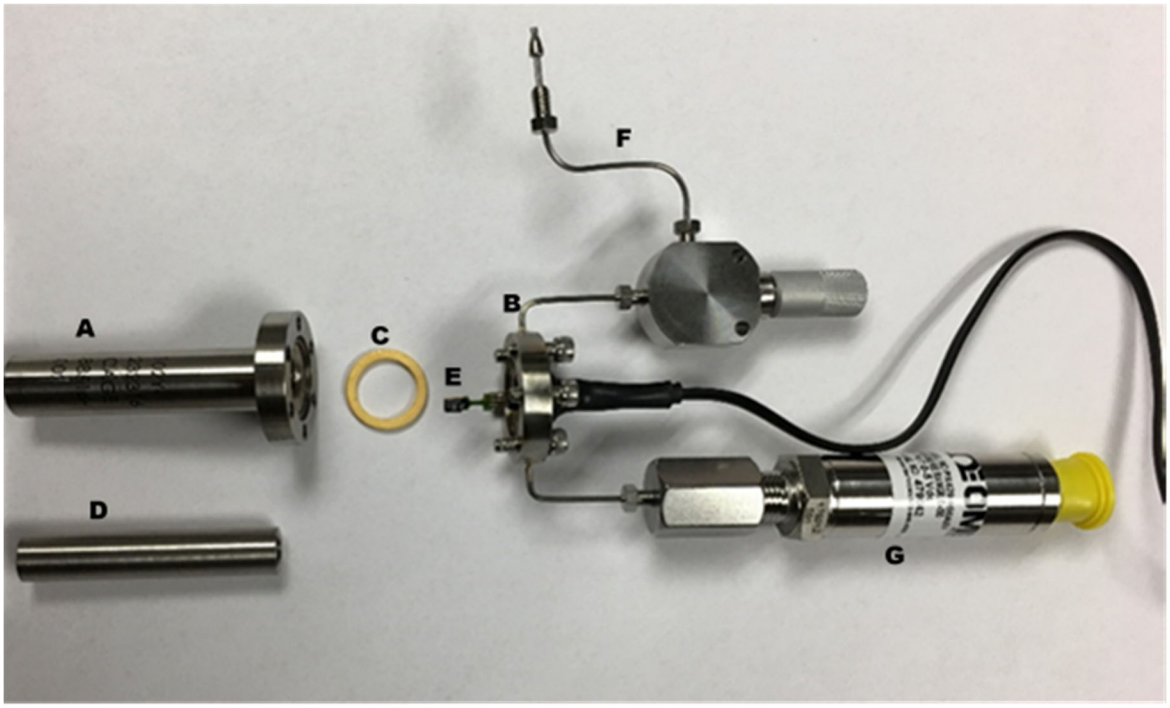

Figure 32. Disassembled example of a Type C SSR: Conflat container body (A) with Conflat flange lid (B), copper gasket (C), inner bucket (D); and RH sensor (E), and a sampling volume between two sampling valves with connection to the gas manifold (F), Omega absolute pressure transducer (G).

Appendix B: Experimental Details for Small-Scale Shelf-Life Studies

The gas generation behavior of MIS represented materials was characterized at the bounding moisture content of 0.5 wt. %. The moisture content was achieved by exposing the material to a humid atmosphere inside the static enclosure surrounding a balance. The duration of the exposure to the humid atmosphere ranged from minutes to hours. Other studies characterized gas generation for materials equilibrated at a specific RH at which the moisture content is determined by the specific properties of the material (e.g. specific surface area, salt content, etc.). The moisture content for those experiments was achieved by equilibration inside constant humidity cells (CHCs) in which the RH was controlled by a saturated salt solution.

The procedure for moisture addition using the humidified balance included (1) estimating the moisture content of the material as it was received for small-scale loading and (2) adding sufficient water to bring the total moisture to the desired set point (0.5 wt.% for MIS represented materials).[20] The initial moisture content of the material was estimated by a LOH-200 °C measurement of a one-gram sample that was removed from the parent lot at the same time as the ~10 g small-scale sample. The LOH-200 °C samples were placed in a glass vial which remained in the glove box line with the small-scale sample until the LOH-200 °C measurement was performed, typically one day or less after the sample split and just prior to loading the SSR. The LOH-200 °C measurements involved heating one gram of the material for two hours at 200 °C, cooling the material for 10 minutes and determining the mass difference of the material before and after heating. The mass loss observed was attributed to adsorbed water. The amount of water to be added was calculated as the difference between 0.5 wt. % and the adsorbed water determined by LOH-200 °C. An additional option for the moisture measurement was Thermal Gravimetric Analysis-Mass Spectroscopy (TGA-MS). TGA-MS is inherently more accurate than LOH-200 °C, although there can be errors associated with this method due to handling and excessive times before the sample is run. When TGA-MS was used, additional samples were removed from the parent material and placed in a hermetically sealed container. After sampling, the material to be loaded in the SSR was placed on the balance with the humidified static enclosure. The weight gain was recorded as a function of time. Once the sample reached the desired set point, the sample was then weighed on a separate high precision balance and immediately transferred to an SSR and sealed. The gloveboxes used for loading and surveillance were flushed with helium, resulting in a glove box atmosphere of mainly helium with a small amount of air. Some moisture loss is expected during the transfer from the humidified chamber into the SSR in the very dry glove box atmosphere (RH < 0.1 %). Transfer time from the balance, where the final mass measurement is made to when the SSR is sealed, is kept to approximately 60 seconds.

The procedure for moisture addition using the CHC included (1) calcination to removed adsorbed species including water and (2) equilibrating the sample with a humidified atmosphere.[28] To remove the previously adsorbed water and other species, the entire sample was heated in a muffle furnace. The calcination temperature ranged from 200 to 950 °C depending on the desired physical characteristics of the material. After calcination, the sample was placed into the inner bucket, and the loaded inner bucket was placed into one arm of a CHC shown in Figure 33. A saturated solution was placed in the other arm of the CHC, and the lids of both arms were closed and sealed. The water vapor from the saturated solution travels through the glass frit separating the arms, and both arms reach the equilibrium RH within several hours. The sample is then left for 7 to 14 days to ensure that it is completely equilibrated with the humidified atmosphere inside the CHC. Once the sample was exposed for the desired amount of time, the sample was then weighed on a separate high precision balance and immediately transferred to an SSR and sealed. Transfer time from the balance, where the final mass measurement is made to when the SSR is sealed, is kept to approximately 60 seconds.

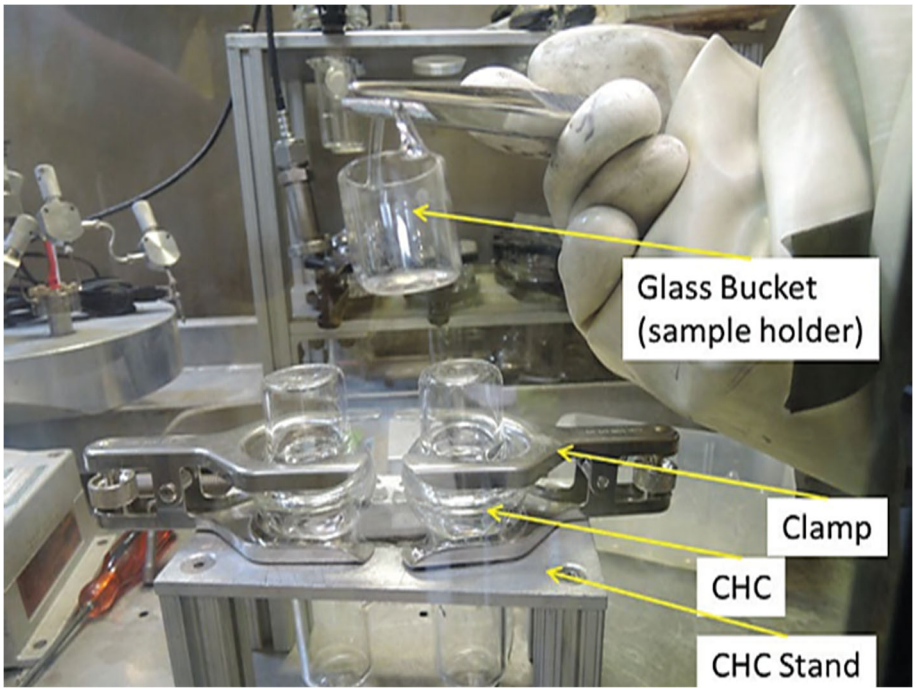

Figure 33. CHC used for equilibration of samples with a humidified atmosphere.

Sealed SSRs were placed in the sample array. The sample array is heated and allows the SSRs to be maintained at specific temperatures or at room temperature depending on the test parameters. MIS represented materials were maintained at 55 °C for the duration of the experiment. Fifty microliter gas samples (~1.1 % of the headspace gas per sample) are extracted periodically through a gas manifold and analyzed using an Agilent 5890 or 7890 gas chromatograph (GC) calibrated for helium, hydrogen, nitrogen, oxygen, carbon dioxide, carbon monoxide and nitrous oxide. Relative humidity (and water vapor) were measured for samples loaded in SSRs with lids that included RH sensors.

When the small-scale experiments are completed, a final GC is taken, and the SSR is removed from the array and allowed to cool to the glovebox temperature. The SSR lid is removed and a new lid containing a Vaisala HMT333 RH sensor is placed on the container. After allowing some time for the system to equilibrate, the RH and temperature in the container is recorded. The material is then removed from the container and the moisture content in the material was determined by performing a LOH-200 °C or a TGA-MS measurement on the sample.

Table 6. List of MIS Represented Items and Loading Conditions.

SSR	MIS Item	Packaging Site	Material Description	Behavior Class	Calcination Condition (% of Total)					Calcination at Loading	Pu	U
					AR	600 °C	750 °C	800 °C	950 °C		(wt. %)	(wt. %)
122	07161856	RFETS	Peroxide Precipitation Product	High-Purity Oxide	13.7%	0.0%	0.0%	0.0%	86.3%	none	84.20	0.0
122A	07161856	RFETS	Peroxide Precipitation Product	High-Purity Oxide	0.0%	0.0%	0.0%	0.0%	100.0%	950 °C	84.20	0.0
123	TS707001	RFETS	Metal Oxidation	High-Purity Oxide	0.0%	0.0%	0.0%	0.0%	100.0%	none	84.20	0.0
124	5501579	RFETS	Pu/U Oxide from Hydride Operation	High-Purity Oxide	0.0%	0.0%	0.0%	0.0%	100.0%	none	88.00	0.4
124A	5501579	RFETS	Pu/U Oxide from Hydride Operation	High-Purity Oxide	0.0%	0.0%	0.0%	0.0%	100.0%	400 °C	88.00	0.4
125	MT1490	RFETS	Metal Oxidation Pu/Np	High-Purity Oxide	7.9%	0.0%	0.0%	46.6%	45.4%	none	87.20	0.0
125A	MT1490	RFETS	Metal Oxidation Pu/Np	High-Purity Oxide	0.0%	0.0%	0.0%	0.0%	100.0%	950 °C	87.20	0.0
125B	MT1490	RFETS	Metal Oxidation Pu/Np	High-Purity Oxide	0.0%	0.0%	0.0%	0.0%	100.0%	950 °C	87.20	0.0
126	669194	RFETS	Pu/U Oxide Miscellaneous	High-Purity Oxide	8.1%	45.6%	0.0%	0.0%	46.3%	none	12.60	68.5
127	CLLANL025	RFETS	Oxide from Pyrochemical Processes	Salt-Bearing Impure Oxide	0.0%	0.0%	100.0%	0.0%	0.0%	750 °C	77.70	0.0
128	07242201A	RFETS	Dissolution Residues	Non-Salt Impure Oxide	0.4%	0.0%	0.0%	0.0%	99.6%	none	63.72	0.0
129	5501407	RFETS	Pu/U Oxide from Hydride Operation	Non-Salt Impure Oxide	60.2%	0.0%	0.0%	0.0%	39.8%	none	65.70	11.7
129A	5501407	RFETS	Pu/U Oxide from Hydride Operation	Non-Salt Impure Oxide	0.0%	0.0%	0.0%	0.0%	100.0%	950 °C	65.70	11.7
130	C06032A	RFETS	Screenings from Oxide (Pyrochemical)	Salt-Bearing Impure Oxide	0.0%	0.0%	0.0%	0.0%	100.0%	950 °C	65.90	0.0
131	ARF-102-85-223	Hanford	Oxide from Pyrochemical Processes	Salt-Bearing Impure Oxide	0.0%	0.0%	100.0%	0.0%	0.0%	750 °C	64.20	0.0
132	BLO-39-11-14-004	Hanford	Oxalate Precipitation Product	High-Purity Oxide	0.0%	0.0%	0.0%	0.0%	100.0%	none	80.00	0.0
132A	BLO-39-11-14-004	Hanford	Oxalate Precipitation Product	High-Purity Oxide	0.0%	0.0%	0.0%	0.0%	100.0%	none	80.00	0.0
133	PSU-84-06-05	Hanford	Pu/U Oxide from Polycube Oxidation	High-Purity Oxide	0.0%	0.0%	0.0%	0.0%	100.0%	none	13.40	65.1
134	66-01-01-439	Hanford	Oxide from Magnesium Hydroxide Precipitation	Non-Salt Impure Oxide	0.0%	0.0%	0.0%	0.0%	100.0%	none	63.70	0.0
135	SCP711-56	LANL	Pu/U Oxide from Fuel Pellets	High-Purity Oxide	0.0%	0.0%	0.0%	0.0%	100.0%	none	17.20	65.7
136	1000089	RFETS	Peroxide Precipitation Product	High-Purity Oxide	7.1%	0.0%	0.0%	47.4%	45.6%	none	84.60	0.0
136A	1000089	RFETS	Peroxide Precipitation Product	High-Purity Oxide	0.0%	0.0%	0.0%	0.0%	100.0%	950 °C	84.60	0.0
137	011589A	RFETS	Metal Oxidation	Salt-Bearing Impure Oxide	0.0%	0.0%	0.0%	0.0%	100.0%	none	77.70	0.0
137A	011589A	RFETS	Metal Oxidation	Salt-Bearing Impure Oxide	0.0%	0.0%	0.0%	0.0%	100.0%	none	77.70	0.0
138	053038	RFETS	By-product Pu/U Oxide	Salt-Bearing Impure Oxide	13.4%	0.0%	0.0%	0.0%	86.6%	none	60.80	3.0
139	520610020	RFETS	Oxide from Pyrochemical Processes	Salt-Bearing Impure Oxide	0.0%	0.0%	91.8%	8.2%	0.0%	none	70.00	0.0
140	07242165A	RFETS	Dissolution Residues	Non-Salt Impure Oxide	0.0%	0.0%	0.0%	8.3%	91.7%	none	34.10	0.0

Appendix B: Experimental Details for Small-Scale Shelf-Life Studies

SSR	MIS Item	Packaging Site	Material Description	Behavior Class	Calcination Condition (% of Total)					Calcination at Loading	Pu	U
					AR	600 °C	750 °C	800 °C	950 °C		(wt. %)	(wt. %)
141	07242141A	RFETS	Oxide Screenings	Non-Salt Impure Oxide	0.0%	0.0%	0.0%	0.0%	100.0%	none	63.10	0.0
142	PBO-47-09-012-023	Hanford	Oxalate Precipitation Product	High-Purity Oxide	0.0%	0.0%	0.0%	0.0%	100.0%	950 °C	87.50	0.0
143	ARF-102-85-355	Hanford	Oxide from Pyrochemical Processes (RFETS)	Salt-Bearing Impure Oxide	0.0%	14.7%	85.3%	0.0%	0.0%	750 °C	70.20	0.0
144	ARF-102-85-365	Hanford	Oxide from Pyrochemical Processes (RFETS)	Salt-Bearing Impure Oxide	0.0%	0.0%	100.0%	0.0%	0.0%	750 °C	58.90	0.0
145	64-85-12-1858	Hanford	Scrap Oxide Miscellaneous	Non-Salt Impure Oxide	0.0%	0.0%	0.0%	0.0%	100.0%	none	32.70	0.0
146	66-00-11-355	Hanford	Oxide from Magnesium Hydroxide Precipitation	Non-Salt Impure Oxide	0.0%	0.0%	0.0%	0.0%	100.0%	none	28.40	0.0
147	CAN92	RFETS	Pu/U Oxide Miscellaneous	High-Purity Oxide	0.0%	0.0%	0.0%	0.0%	100.0%	none	83.57	1.9
148	C00024A	RFETS	Oxide from Pyrochemical Processes	Salt-Bearing Impure Oxide	2.3%	0.0%	0.0%	0.0%	97.7%	none	73.30	0.0
149D	C00695	RFETS	Oxide from Pyrochemical Processes	Salt-Bearing Impure Oxide	7.5%	0.0%	0.0%	44.6%	47.9%	none	74.10	0.0
150	TS707013	RFETS	Metal Oxidation	Salt-Bearing Impure Oxide	0.0%	0.0%	0.0%	0.0%	100.0%	none	69.80	0.0
151A	07032282A	RFETS	Dissolution Residues	Salt-Bearing Impure Oxide	0.0%	0.0%	0.0%	0.0%	100.0%	none	67.90	0.0
152	41-85-08-1379	Hanford	Scrap Oxide Miscellaneous	Non-Salt Impure Oxide	0.0%	0.0%	0.0%	0.0%	100.0%	none	44.90	0.0
153D	63-88-06-121	Hanford	Scrap Oxide Miscellaneous	Non-Salt Impure Oxide	0.0%	0.0%	0.0%	0.0%	100.0%	none	35.10	0.0
154	ARF-102-85-114-1	Hanford	Metal Oxidation (RFETS)	High-Purity Oxide	0.0%	0.0%	0.0%	0.0%	100.0%	none	86.30	0.0
155	ARF-102-85-295	Hanford	Oxide from Pyrochemical Processes (RFETS)	Salt-Bearing Impure Oxide	0.0%	0.0%	100.0%	0.0%	0.0%	750 °C	40.00	0.0
155HT	ARF-102-85-295	Hanford	Oxide from Pyrochemical Processes (RFETS)	Salt-Bearing Impure Oxide	6.7%	0.8%	0.0%	0.0%	92.5%	none	40.00	0.0
156	PuF4-1	LANL	Plutonium Fluoride Precipitation	Non-Salt Impure Oxide	0.0%	0.0%	0.0%	0.0%	100.0%	none	55.10	0.0
160	PMAXBS	LANL	Oxide from Pyrochemical Processes	Salt-Bearing Impure Oxide	0.0%	0.0%	0.0%	100.0%	0.0%	none	71.80	0.0
161	PEOF1	LANL	Oxalate Precipitation Product	High-Purity Oxide	0.0%	0.0%	0.0%	0.0%	100.0%	none	87.20	0.0
162	MISSTD-1	LANL	Oxalate Precipitation Product	High-Purity Oxide	0.0%	100.0%	0.0%	0.0%	0.0%	none	85.96	0.0
203A	CXLPROD091901	LANL	Oxalate Precipitation Product	High-Purity Oxide	0.0%	0.0%	0.0%	0.0%	100.0%	none	87.01	0.0
204	CXLPROD021202	LANL	Oxalate Precipitation Product	High-Purity Oxide	0.0%	0.0%	0.0%	0.0%	100.0%	none	87.44	0.1
205	CXLOX091802A	LANL	Oxalate Precipitation Impure	Salt-Bearing Impure Oxide	0.0%	0.0%	0.0%	0.0%	100.0%	none	78.30	0.0
207	04272-CC-220-AS	LANL	Unknown; Contains thorium	Non-Salt Impure Oxide	0.0%	0.0%	0.0%	0.0%	100.0%	none	83.10	0.0
208A	04272-CC-220-AS	LANL	Unknown; Contains thorium	Non-Salt Impure Oxide	0.0%	0.0%	0.0%	0.0%	100.0%	none	83.10	0.0
232	CXLOX022411-S3	LANL	Oxalate Precipitation Impure	Non-Salt Impure Oxide	0.0%	0.0%	0.0%	0.0%	100.0%	none	65.00	0.0
232A	CXLOX022411-S3	LANL	Oxalate Precipitation Impure	Non-Salt Impure Oxide	0.0%	0.0%	0.0%	0.0%	100.0%	none	65.00	0.0

Appendix B: Experimental Details for Small-Scale Shelf-Life Studies

SSR	MIS Item	Packaging Site	Material Description	Behavior Class	Calcination Condition (% of Total)					Calcination at Loading	Pu	U
					AR	600 °C	750 °C	800 °C	950 °C		(wt. %)	(wt. %)
233	H003328	Hanford	Oxide from Pyrochemical Processes (RFETS)	Salt-Bearing Impure Oxide	100.0%	0.0%	0.0%	0.0%	0.0%	none	74.90	0.0
233B	H003328	Hanford	Oxide from Pyrochemical Processes (RFETS)	Salt-Bearing Impure Oxide	100.0%	0.0%	0.0%	0.0%	0.0%	none	74.90	0.0
234	H003328	Hanford	Oxide from Pyrochemical Processes (RFETS)	Salt-Bearing Impure Oxide	100.0%	0.0%	0.0%	0.0%	0.0%	none	74.90	0.0
231	UPOPLOT0003-MIS	LANL	Metal Oxidation (ARIES Oxide)	High-Purity Oxide	0.0%	0.0%	0.0%	0.0%	100.0%	none	86.90	0.0
235	UPOPLOT0003-MIS	LANL	Metal Oxidation (ARIES Oxide)	High-Purity Oxide	0.0%	0.0%	0.0%	0.0%	100.0%	none	86.90	0.0
235A	UPOPLOT0003-MIS	LANL	Metal Oxidation (ARIES Oxide)	High-Purity Oxide	0.0%	0.0%	0.0%	0.0%	100.0%	950 °C	86.90	0.0
235B	UPOPLOT0003-MIS	LANL	Metal Oxidation (ARIES Oxide)	High-Purity Oxide	0.0%	0.0%	0.0%	0.0%	100.0%	none	86.90	0.0

Appendix B: Experimental Details for Small-Scale Shelf-Life Studies

Table 7. List of Chloride-Bearing Impure Oxides Included in This Report.

SSR	MIS Item	Packaging Site	Material Description	Calcination Condition (% of Total)					Calcination at Loading	Pu	U	Hydration Method	H_2O	Report
				AR	600 °C	750 °C	800 °C	950 °C		(wt%)	(wt%)		(wt%)	LA-UR
127	CLLANL025	RFETS	Oxide from Pyrochemical Processes	0.0%	0.0%	100.0%	0.0%	0.0%	750 °C	77.7	0.0	Humidified Balance	0.45	
150	TS707013	RFETS	Metal Oxidation	0.0%	0.0%	0.0%	0.0%	100.0%	950 °C	33.9	0.0	Humidified Balance	0.53	22-20058
139	520610020	RFETS	Oxide from Pyrochemical Processes	0.0%	0.0%	91.8%	8.2%	0.0%	none	70.0	0.0	Humidified Balance	0.45	20-29362
148	C00024A	RFETS	Oxide from Pyrochemical Processes	2.3%	0.0%	0.0%	0.0%	97.7%	none	71.5	0.0	Humidified Balance	0.53	
130	C06032A	RFETS	Screenings from Oxide (Pyrochemical)	0.0%	0.0%	0.0%	0.0%	100.0%	950 °C	65.9	0.0	Humidified Balance	0.51	
155	ARF-102-85-295	HANFORD	Oxide from Pyrochemical Processes (RFETS)	0.0%	0.0%	100.0%	0.0%	0.0%	750 °C	26.3	0.0	Humidified Balance	0.80	
149D	C00695	RFETS	Oxide from Pyrochemical Processes	7.5%	0.0%	0.0%	44.6%	47.9%	none	73.9	0.0	Humidified Balance	0.58	
137	011589A	RFETS	Metal Oxidation	0.0%	0.0%	0.0%	0.0%	100.0%	none	77.7	0.0	Humidified Balance	0.52	
138	053038	RFETS	By-product Pu-U Oxide	13.4%	0.0%	0.0%	0.0%	86.6%	none	60.8	3.0	Humidified Balance	0.78	
233B	H003328	Hanford	Oxide from Pyrochemical Processes (RFETS)	100.0%	0.0%	0.0%	0.0%	0.0%	none	74.9	0.0	Humidified Balance	0.60	
233	H003328	Hanford	Oxide from Pyrochemical Processes (RFETS)	100.0%	0.0%	0.0%	0.0%	0.0%	none	74.9	0.0	Humidified Balance	0.27	
160	PMAXBS	LANL	Oxide from Pyrochemical Processes	0.0%	0.0%	0.0%	100.0%	0.0%	none	71.8	0.0	Humidified Balance	0.19	
233B	H003328	Hanford	Oxide from Pyrochemical Processes (RFETS)	100.0%	0.0%	0.0%	0.0%	0.0%	none	74.9	0.0	Humidified Balance	0.60	
233	H003328	Hanford	Oxide from Pyrochemical Processes (RFETS)	100.0%	0.0%	0.0%	0.0%	0.0%	none	74.9	0.0	Humidified Balance	0.27	
160	PMAXBS	LANL	Oxide from Pyrochemical Processes	0.0%	0.0%	0.0%	100.0%	0.0%	none	71.8	0.0	Humidified Balance	0.19	

Appendix B: Experimental Details for Small-Scale Shelf-Life Studies

Table 8. List of High-Purity Oxides Included in This Report.

SSR	MIS Item	Packaging Site	Material Description	Calcination Condition (% of Total)					Calcination at Loading	Pu	U	Hydration Method	H_2O	Report
				AR	600 °C	750 °C	800 °C	950 °C		(wt%)	(wt%)		(wt%)	LA-UR
122	07161856	RFETS	Peroxide Precipitation Product	13.7%	0.0%	0.0%	0.0%	86.3%	none	84.20	0.00	Humidified Balance	0.690	21-30452
123	TS707001	RFETS	Metal Oxidation	0.0%	0.0%	0.0%	0.0%	100.0%	none	84.20	0.00	Humidified Balance	0.270	21-30452
125	MT1490	RFETS	Metal Oxidation Pu/Np	7.9%	0.0%	0.0%	46.6%	45.4%	none	87.20	0.00	Humidified Balance	0.400	19-20523
125A	MT1490	RFETS	Metal Oxidation Pu/Np	0.0%	0.0%	0.0%	0.0%	100.0%	950 °C	87.20	0.00	Humidified Balance	0.087	
125B	MT1490	RFETS	Metal Oxidation Pu/Np	0.0%	0.0%	0.0%	0.0%	100.0%	950 °C	87.20	0.00	Humidified Balance	0.063	
132A	BLO-39-11-14-004	Hanford	Oxalate Precipitation Product	0.0%	0.0%	0.0%	0.0%	100.0%	none	80.00	0.00	Humidified Balance	0.590	18-26650
136A	1000089	RFETS	Peroxide Precipitation Product	0.0%	0.0%	0.0%	0.0%	100.0%	950 °C	84.60	0.00	Humidified Balance	0.100	22-24447
142	PBO-47-09-012-023	Hanford	Oxalate Precipitation Product	0.0%	0.0%	0.0%	0.0%	100.0%	950 °C	87.50	0.00	Humidified Balance	0.500	19-31446
154	ARF-102-85-114-1	Hanford	Metal Oxidation (RFETS)	0.0%	0.0%	0.0%	0.0%	100.0%	950 °C	86.32	0.00	Humidified Balance	0.450	
213	PEOF1	LANL	Oxalate Precipitation Product	0.0%	0.0%	0.0%	0.0%	100.0%	400 °C	87.20	0.00	Constant Humidity Cell	0.046	19-24622
218	PEOF1	LANL	Oxalate Precipitation Product	0.0%	0.0%	0.0%	0.0%	100.0%	400 °C	87.20	0.00	Constant Humidity Cell	0.069	19-24622
236	BLO-39-11-14-004	Hanford	Oxalate Precipitation Product	0.0%	0.0%	0.0%	0.0%	100.0%	400 °C	80.00	0.00	Constant Humidity Cell	0.387	19-24622
237	BLO-39-11-14-004	Hanford	Oxalate Precipitation Product	0.0%	0.0%	0.0%	0.0%	100.0%	400 °C	80.00	0.00	Constant Humidity Cell	0.595	19-24622
239	PEOF1	LANL	Oxalate Precipitation Product	0.0%	0.0%	0.0%	0.0%	100.0%	400 °C	87.20	0.00	Constant Humidity Cell	0.046	19-24622
240A	PEOF1	LANL	Oxalate Precipitation Product	0.0%	0.0%	0.0%	0.0%	100.0%	400 °C	87.20	0.00	Constant Humidity Cell	0.054	19-24622
242	PEOF1	LANL	Oxalate Precipitation Product	0.0%	0.0%	0.0%	0.0%	100.0%	400 °C	87.20	0.00	Constant Humidity Cell	0.265	19-24622
243	PEOF1	LANL	Oxalate Precipitation Product	0.0%	0.0%	0.0%	0.0%	100.0%	400 °C	87.20	0.00	Constant Humidity Cell	1.066	19-24622
244	MISSTD-1	LANL	Oxalate Precipitation Product	0.0%	100.0%	0.0%	0.0%	0.0%	600 °C	85.96	0.00	Constant Humidity Cell	1.049	19-24622
245	MISSTD-1	LANL	Oxalate Precipitation Product	0.0%	100.0%	0.0%	0.0%	0.0%	600 °C	85.96	0.00	Constant Humidity Cell	1.193	19-24622

Appendix B: Experimental Details for Small-Scale Shelf-Life Studies

SSR	MIS Item	Packaging Site	Material Description	Calcination Condition (% of Total)					Calcination at Loading	Pu	U	Hydration Method	H_2O	Report
				AR	600 °C	750 °C	800 °C	950 °C		(wt%)	(wt%)		(wt%)	LA-UR
246	MISSTD-1	LANL	Oxalate Precipitation Product	0.0%	100.0%	0.0%	0.0%	0.0%	600 °C	85.96	0.00	Constant Humidity Cell	1.338	19-24622
247	MISSTD-1	LANL	Oxalate Precipitation Product	0.0%	100.0%	0.0%	0.0%	0.0%	600 °C	85.96	0.00	Constant Humidity Cell	1.824	19-24622
248	MISSTD-1	LANL	Oxalate Precipitation Product	0.0%	100.0%	0.0%	0.0%	0.0%	600 °C	85.96	0.00	Constant Humidity Cell	1.800	19-24622
249	BLO-39-11-14-004	Hanford	Oxalate Precipitation Product	0.0%	100.0%	0.0%	0.0%	0.0%	400 °C	80.00	0.00	Constant Humidity Cell	0.591	19-24622
251	AAP02OX	LANL	Metal Oxidation	100.0%	0.0%	0.0%	0.0%	0.0%	400 °C	86.00	0.50	Constant Humidity Cell	0.397	18-28416
256	BLO-39-11-14-004	Hanford	Oxalate Precipitation Product	0.0%	0.0%	0.0%	0.0%	100.0%	950 °C	80.00	0.00	Constant Humidity Cell	0.058	19-24622
257	BLO-39-11-14-004	Hanford	Oxalate Precipitation Product	0.0%	0.0%	0.0%	0.0%	100.0%	950 °C	80.00	0.00	Constant Humidity Cell	0.074	19-24622
258	BLO-39-11-14-004	Hanford	Oxalate Precipitation Product	0.0%	0.0%	0.0%	0.0%	100.0%	950 °C	80.00	0.00	Constant Humidity Cell	0.104	19-24622
265B	LAO225BS	LANL	Peroxide Precipitation Product	0.0%	0.0%	100.0%	0.0%	0.0%	750 °C	87.52	0.00	Constant Humidity Cell	0.273	
266A	LAO225BS	LANL	Peroxide Precipitation Product	0.0%	0.0%	100.0%	0.0%	0.0%	750 °C	87.52	0.00	Constant Humidity Cell	0.387	
267A	LAO225BS	LANL	Peroxide Precipitation Product	0.0%	0.0%	100.0%	0.0%	0.0%	750 °C	87.52	0.00	Constant Humidity Cell	0.534	
124	5501579	RFETS	Pu/U Oxide from Hydride Operation	0.0%	0.0%	0.0%	0.0%	100.0%	none	88.00	0.40	Humidified Balance	0.330	18-20970
124A	5501579	RFETS	Pu/U Oxide from Hydride Operation	0.0%	0.0%	0.0%	0.0%	100.0%	400 °C	88.00	0.40	Humidified Balance	0.230	18-20970
126	669194	RFETS	Pu/U Oxide Miscellaneous	8.1%	45.6%	0.0%	0.0%	46.3%	none	12.60	68.50	Humidified Balance	0.310	22-30655
129	5501407	RFETS	Pu/U Oxide from Hydride Operation	60.2%	0.0%	0.0%	0.0%	39.8%	none	65.70	11.72	Humidified Balance	0.820	19-20826
135	SCP711-56	LANL	Pu/U Oxide from Fuel Pellets	0.0%	0.0%	0.0%	0.0%	100.0%	none	17.20	65.70	Humidified Balance	0.060	19-20356
147	CAN92	RFETS	Pu/U Oxide Miscellaneous	0.0%	0.0%	0.0%	0.0%	100.0%	none	83.57	1.89	Humidified Balance	0.430	22-29337